AIAA JOURNAL
Vol. 45, No. 9, September 2007

Compact, Generalized Component Mode Mistuning Representation for Modeling Bladed Disk Vibration

Sang-Ho Lim,* Ronnie Bladh,† and Matthew P. Castanier‡
University of Michigan, Ann Arbor, Michigan 48109-2125
and
Christophe Pierre§
McGill University, Montreal, Quebec H3A 2K6, Canada

DOI: 10.2514/1.13172

New techniques are presented for generating reduced-order models of the vibration of mistuned bladed disks from parent finite element models. A novel component-based modeling framework is developed by partitioning the system into a tuned bladed disk component and virtual blade mistuning components. The mistuning components are defined by the differences between the mistuned and tuned blade mass and stiffness matrices. The mistuned-system model is assembled with a component mode synthesis technique, using a basis of tuned-system normal modes and attachment modes. The formulation developed is general and can be applied to any mistuned bladed disk, including those with large geometric mistuning (e.g., severe blade damage). In the case of small (i.e., blade frequency) mistuning, a compact reduced-order model is derived by neglecting the attachment modes. For this component mode mistuning model, the blade mistuning is projected first onto the component modes of a tuned, cantilevered blade, and then projected again onto the tuned-system normal modes via modal participation factors. In this manner, several natural frequencies of each mistuned blade can be used to capture systematically the effects of the complex physical sources of mistuning. A numerical validation of the developed methods is performed for both large and small mistuning cases using a finite element model of an industrial rotor.

Nomenclature

$\boldsymbol{c}$	=	aerodynamic coupling damping matrix projected onto tuned-system normal modes
E	=	Young's modulus
$\boldsymbol{F}$	=	real Fourier matrix
$\boldsymbol{f}$	=	excitation force vector
j	=	$\sqrt{-1}$
$\boldsymbol{K}$	=	stiffness matrix in physical coordinates
$\boldsymbol{M}$	=	mass matrix in physical coordinates
N	=	no. of blades
N_h	=	no. of the retained tuned-system normal modes corresponding to harmonic h
$\boldsymbol{p}$	=	modal coordinates
$\boldsymbol{q}$, $\tilde{\boldsymbol{q}}_h$	=	set of tuned-cantilevered-blade mode participation factors for the blade motion in the retained tuned-system modes in physical coordinates and in cyclic coordinates
$\boldsymbol{U}$	=	set of the retained tuned-cantilevered-blade normal and boundary modes
v, $\boldsymbol{v}$	=	mistuned-cantilevered-blade normal mode participation factor for a tuned-cantilevered-blade normal mode and set of the factors
$\boldsymbol{x}$	=	physical coordinates
γ	=	structural damping coefficient
δ	=	nondimensional mistuning parameter
$\boldsymbol{\kappa}$	=	reduced stiffness matrix or stiffness projection to the retained component modes
λ, $\boldsymbol{\Lambda}$	=	eigenvalue and diagonal matrix of eigenvalues of the retained component normal modes
$\boldsymbol{\mu}$	=	reduced mass matrix or mass projection to the retained component modes
$\boldsymbol{\Phi}$, $\tilde{\boldsymbol{\Phi}}$	=	set of the retained component normal modes in physical coordinates and in cyclic coordinates
$\boldsymbol{\Psi}$	=	component interface modes
ω	=	frequency

Subscripts

b, i	=	finite element degrees of freedom (DOF) of the cantilevered-blade boundary and interior
H	=	maximum harmonic number
h	=	harmonic number
n	=	blade number
o	=	tuned blade
$\boldsymbol{R}$	=	set of the retained cantilevered-blade normal mode numbers
r	=	rth cantilevered-blade normal mode
Γ	=	finite element DOF of the blades
Δ	=	finite element DOF of the disk
Φ	=	generalized coordinates for the retained component normal modes
ϕ	=	partition for cantilevered-blade normal modes
Ψ	=	generalized coordinates for the component interface modes
ψ	=	partition for cantilevered-blade boundary modes

Superscripts

a	=	aerodynamic coupling

Presented as Paper 1545 at the 44th AIAA/ASME/ASCE/AHS/ASC Structures, Structural Dynamics and Materials Conference, Norfolk, Virginia, 7–10 April 2003; received 31 August 2004; revision received 23 February 2007; accepted for publication 24 February 2007.

*Graduate Student, Department of Mechanical Engineering; currently Senior Research Engineer, Samsung Corning Precision Glass, Finishing Technology Lab, Asan-City, ChungNam 336-840, South Korea.

†Visiting Research Investigator, Department of Mechanical Engineering; currently Senior Engineer, Siemens Industrial Turbomachinery AB, Research and Development, Department GRCRM, SE-61283 Finspong, Sweden.

‡Associate Research Scientist, Department of Mechanical Engineering. Senior Member AIAA.

§Dean, Faculty of Engineering. Senior Member AIAA.

B	=	cantilevered blade
E	=	Young's modulus mistuning
e	=	eigenvalue mistuning
k	=	modes or modal participation factors for stiffness mistuning
m	=	modes or modal participation factors for mass mistuning
S	=	tuned system
syn	=	synthesized representation
δ	=	mistuning component or assembly of mistuning components

Introduction

A BLADED disk consists of a set of disk-blade sectors that are typically designed to be identical. In practice, however, there are always small variations in the structural properties of individual blades, resulting from manufacturing tolerances, material deviations, and operational wear. These variations are referred to as blade mistuning. Because of mistuning, the vibratory response of an industrial bladed disk may be considerably different from that of its nominal, tuned design. In particular, some blades may have much higher forced response levels due to mistuning. Over the past 40 years much research has been done on the dynamic behavior of mistuned bladed disks [1–3], and many of these studies have been based on lumped parameter models [4–12]. Although such simple models do provide a basic understanding of the effects of mistuning, they usually cannot be used to predict accurately the vibratory response of industrial bladed disks. On the other hand, because mistuning is random, a probabilistic analysis such as a Monte Carlo simulation is needed, and the computational cost makes it impractical to use finite element models directly. Therefore, various techniques have been developed to construct reduced-order models of bladed disks systematically from their finite element representations. These techniques include component mode synthesis or related methods [13–19], a receptance technique [20], and classical modal analysis with a mistuning projection [21]. The major differences among these reduced-order modeling techniques are the substructuring approaches and the mistuning implementations. Another method to obtain the response of mistuned systems without building an attendant reduced-order model has been proposed by Petrov et al. [22]. In this approach, the response of a mistuned system is calculated using response levels for the tuned assembly, together with a modification matrix constructed from the frequency response function matrix of the tuned system and a matrix describing the mistuning.

In many methods developed to date, reduced-order models are obtained by substructuring a bladed disk into disk and blade components, because this allows for easy implementation of blade mistuning. However, an alternative approach has been proposed by Yang and Griffin [21], in which the tuned-system normal modes are used without substructuring to generate a reduced-order model. One advantage of avoiding substructuring is that there is no additional error introduced in the tuned-system model. Another advantage is that, because the number of tuned-system normal modes required is on the order of the number of blades, the size of Yang and Griffin's reduced-order model is as small or smaller than that of any other method.

The way in which blade mistuning is implemented into a reduced-order model is a key issue, because mistuned reduced-order models should be able to predict the behavior of actual mistuned systems. Castanier et al. [14] included mistuning in a component-based reduced-order model by varying the blade modal stiffnesses that appear explicitly in a synthesized stiffness matrix. Bladh et al. [15] extended this method by projecting mistuning onto the normal modes of a tuned cantilevered blade fixed at the disk-blade interface. Because a small number of modal stiffness variations are directly employed in the reduced-order model, the implementation of mistuning is quite efficient. Also, because different mistuning patterns can be used for the various individual blade modes, bladed disks can be modeled more realistically. Therefore, this mistuning projection method has great potential for general implementation in reduced-order models. Yang and Griffin [21] used a similar mistuning projection, but in theory their method requires the knowledge of the mistuned mass and stiffness matrices in physical coordinates, because the mistuning expressed in physical coordinates is directly projected to the tuned-system modes. Therefore, they only considered the case in which a mistuned blade stiffness matrix is proportional to the tuned matrix. The method proposed by Petrov et al. [22] also uses a mistuning matrix in physical coordinates. Therefore, for the practical implementation of mistuning, it is clear that the mistuning projection method of Bladh et al. [15] is useful, with the caveats that the component mode shapes of mistuned and tuned blades are assumed to be the same and that only stiffness mistuning is present.

In this paper, a general reduced-order model for mistuned bladed disks is developed. In this approach, the mistuned system is represented by the full tuned system and by virtual blade mistuning components, and a hybrid-interface method is used to combine them. The mistuning components consist only of blade mass and stiffness deviations from the tuned configuration, and all the degrees of freedom (DOF) in the mistuning components are considered to be interface degrees of freedom. Because no assumption is made about mistuning in this formulation, the resulting reduced-order model can be constructed for arbitrary mistuning, regardless of whether it is small or large.

Most previous research on mistuning has been based on the assumption that mistuning is small (i.e., small blade-frequency mistuning), which is not necessarily the case. If there is large mistuning, such as a fractured blade tip or significant variations in blade geometry due to damage, then it is necessary to include a very large number of tuned-system modes or tuned-component (disk and blade) modes in the reduced-order models. This is due to the fact that mistuning may change the mass or stiffness matrices significantly. In this case, the mode shapes of a mistuned blade may be very different from those of a tuned blade when comparing them with a metric such as the modal assurance criterion [23,24]. Because of this difficulty, the reduced-order models described above have not been able to capture such large mistuning. In the general formulation proposed in this paper, the attachment modes of the tuned system are used to generate an accurate reduced-order model for the case of large mistuning. This allows for the efficient prediction of the response of bladed disks with large, mode shape mistuning. Furthermore, intentional mistuning [25], which may involve geometric design changes in local areas of the blades, can be efficiently studied with this method.

In this paper, a reduced-order model for the special case of small mistuning is also derived from the general formulation. This model uses the same tuned mode basis, and thus it features the same small number of DOF as that of Yang and Griffin's method [21]. Blade mistuning is implemented using the mistuning projection approach originally developed by Bladh et al. [15], which is extended here to handle the generalized blade mistuning cases considered. By using only a few modes of a mistuned cantilevered blade, any type of small structural mistuning can be accurately accounted for. This new approach to small-mistuned bladed disks is referred to as the component mode mistuning (CMM) method. In preceding studies [15–17], a bladed disk was substructured into disk and blade components to project mistuning to the normal modes of a tuned cantilevered blade. In the proposed CMM method, the mistuning is projected without requiring a component-based representation of the full system.

A major advantage of this method is that, even when mistuning is present in only part of the blade such that the modal mistuning patterns for the various blade modes are different, the influence of mistuning may still be estimated accurately. That is, arbitrary patterns of mistuning in the physical mass and stiffness matrices can be efficiently and accurately implemented in a compact reduced-order model using modal mistuning values for a few cantilevered-blade modes. This feature is especially useful in frequency ranges where two or more families of blade-dominated modes of the tuned system are closely spaced. In such a frequency region, a mistuned-

system mode may exhibit blade motion that is characteristic of multiple types of blade modes. An example of this is shown in one of the numerical case studies.

The primary contribution of this paper is a new method for systematically formulating a general reduced-order model of mistuned bladed disks, regardless of whether mistuning is small or large. In particular, the new reduced-order model handles the effects of large structural and geometric variations, such as damaged blades. Another contribution is the development of a compact modeling framework for a bladed disk with generalized small blade mistuning and aerodynamic coupling. In particular, the CMM model allows one to handle the cases of nonproportional mistuning of the blade stiffness matrix and different mistuning patterns for different blade modes.

The paper is organized as follows. The general formulation of a reduced-order model for a bladed disk with arbitrary mistuning is presented in the second section. The CMM representation for the case of small blade mistuning is derived in the third section. In the fourth section, the general approach is validated by comparing the results of the finite element model (FEM) and the reduced-order model (ROM) for an industrial rotor with a rogue blade, which causes large mistuning. In the fifth section, the CMM approach is validated numerically for the same industrial rotor but with small mistuning. The example cases include mistuning that leads to a proportional change in the blade stiffness matrix as well as nonproportional mistuning. The conclusions are given in the sixth section.

General Reduced-Order Model Formulation for a Mistuned System

A general, component-based framework is considered, in which a mistuned bladed disk is partitioned into a tuned bladed disk component and one virtual component for each blade, as shown in Fig. 1. Each virtual component, or mistuning component, is defined as having mass and stiffness matrices equal to the difference between the mistuned and tuned matrices of a single blade. That is, the mistuning component for blade n has the following mass and stiffness matrices:

$$\boldsymbol{M}_n^{\delta} = \boldsymbol{M}_n - \boldsymbol{M}_o, \qquad \boldsymbol{K}_n^{\delta} = \boldsymbol{K}_n - \boldsymbol{K}_o \tag{1}$$

Note that the mistuning component matrices vanish if the blade is tuned. Because the response of a typical bladed disk is much more sensitive to mistuning in the blades than in the disk, only blade mistuning is considered in this study. However, the proposed substructuring approach could be applied to the disk as well.

To combine the tuned system and mistuning components, a component mode synthesis (CMS) [26–28] approach is employed. More specifically, a hybrid-interface CMS approach is used, where the interface (or active) DOF are all the blade DOF. The tuned system is treated as a free-interface component, whereas the mistuning components are treated as fixed-interface components.

For the tuned-system component, normal modes and attachment modes [28] are needed. Because it is a free-interface component, the component normal modes are simply the modes of the tuned bladed disk. The attachment modes are obtained by applying a unit force to each interface DOF, successively. The reduced mass and stiffness matrices in generalized coordinates for the free-interface component (the tuned system) can be written using its truncated set of normal modes $\boldsymbol{\Phi}^S$ and complete set of attachment modes $\boldsymbol{\psi}^S$ as follows:

$$\boldsymbol{\mu}^S = \begin{bmatrix} \boldsymbol{I} & \boldsymbol{\Phi}^{S^T}\boldsymbol{M}^S\boldsymbol{\Psi}^S \\ \boldsymbol{\Psi}^{S^T}\boldsymbol{M}^S\boldsymbol{\Phi}^S & \boldsymbol{\Psi}^{S^T}\boldsymbol{M}^S\boldsymbol{\Psi}^S \end{bmatrix} \tag{2a}$$

$$\boldsymbol{\kappa}^S = \begin{bmatrix} \boldsymbol{\Lambda}^S & \boldsymbol{\Phi}^{S^T}\boldsymbol{K}^S\boldsymbol{\Psi}^S \\ \boldsymbol{\Psi}^{S^T}\boldsymbol{K}^S\boldsymbol{\Phi}^S & \boldsymbol{\Psi}_{\Gamma}^S \end{bmatrix} \tag{2b}$$

$$\boldsymbol{x}^S = \begin{Bmatrix} \boldsymbol{x}_{\Delta}^S \\ \boldsymbol{x}_{\Gamma}^S \end{Bmatrix} = \begin{bmatrix} \boldsymbol{\Phi}_{\Delta}^S & \boldsymbol{\Psi}_{\Delta}^S \\ \boldsymbol{\Phi}_{\Gamma}^S & \boldsymbol{\Psi}_{\Gamma}^S \end{bmatrix} \begin{Bmatrix} \boldsymbol{p}_{\Phi}^S \\ \boldsymbol{p}_{\Psi}^S \end{Bmatrix} \tag{2c}$$

For a mistuning component, a set of constraint modes [27] are obtained by enforcing a unit displacement at each interface DOF, successively, with all other interface DOF held fixed. Because all the DOF in the mistuning component are interface DOF, and it is treated as a fixed-interface component, there are no component normal modes. Therefore, the set of constraint modes, which in this case is the identity matrix, completely describe the motion of the mistuning component. For the assembly of all blade mistuning components, the mass and stiffness matrices in generalized coordinates are the same as those in physical coordinates:

$$\boldsymbol{\mu}^{\delta} = \boldsymbol{I}^T\boldsymbol{M}^{\delta}\boldsymbol{I} = \boldsymbol{M}^{\delta} = \underset{n=1,\ldots,N}{\mathbf{Bdiag}}\left[\boldsymbol{M}_n^{\delta}\right] \tag{3a}$$

$$\boldsymbol{\kappa}^{\delta} = \boldsymbol{I}^T\boldsymbol{K}^{\delta}\boldsymbol{I} = \boldsymbol{K}^{\delta} = \underset{n=1,\ldots,N}{\mathbf{Bdiag}}\left[\boldsymbol{K}_n^{\delta}\right] \tag{3b}$$

$$\boldsymbol{x}^{\delta} = \boldsymbol{I}\boldsymbol{p}_{\Psi}^{\delta} = \boldsymbol{p}_{\Psi}^{\delta} \tag{3c}$$

where $\underset{n=1,\ldots,N}{\mathbf{Bdiag}}[\cdot]$ denotes a block-diagonal matrix with block n corresponding to blade n.

The synthesis of the tuned system and mistuning components is achieved by satisfying displacement compatibility at the component interface (i.e., $\boldsymbol{x}_{\Gamma}^S = \boldsymbol{x}^{\delta}$). This yields, from Eqs. (2c) and (3c)

$$\boldsymbol{\Phi}_{\Gamma}^S\boldsymbol{p}_{\Phi}^S + \boldsymbol{\Psi}_{\Gamma}^S\boldsymbol{p}_{\Psi}^S = \boldsymbol{p}_{\Psi}^{\delta} \tag{4}$$

This constraint equation leads to the synthesized representation of a mistuned system:

$$[-\omega^2\boldsymbol{\mu}^{\text{syn}} + (1 + j\gamma)\boldsymbol{\kappa}^{\text{syn}}]\boldsymbol{p}^{\text{syn}} = [\boldsymbol{\Phi}^S\boldsymbol{\Psi}^S]^T\boldsymbol{f} \tag{5}$$

where

$$\boldsymbol{\mu}^{\text{syn}} = \boldsymbol{\mu}^S + \begin{bmatrix} \boldsymbol{\Phi}_{\Gamma}^{S^T}\boldsymbol{M}^{\delta}\boldsymbol{\Phi}_{\Gamma}^S & \boldsymbol{\Phi}_{\Gamma}^{S^T}\boldsymbol{M}^{\delta}\boldsymbol{\Psi}_{\Gamma}^S \\ \boldsymbol{\Psi}_{\Gamma}^{S^T}\boldsymbol{M}^{\delta}\boldsymbol{\Phi}_{\Gamma}^S & \boldsymbol{\Psi}_{\Gamma}^{S^T}\boldsymbol{M}^{\delta}\boldsymbol{\Psi}_{\Gamma}^S \end{bmatrix} \tag{6a}$$

$$\boldsymbol{\kappa}^{\text{syn}} = \boldsymbol{\kappa}^S + \begin{bmatrix} \boldsymbol{\Phi}_{\Gamma}^{S^T}\boldsymbol{K}^{\delta}\boldsymbol{\Phi}_{\Gamma}^S & \boldsymbol{\Phi}_{\Gamma}^{S^T}\boldsymbol{K}^{\delta}\boldsymbol{\Psi}_{\Gamma}^S \\ \boldsymbol{\Psi}_{\Gamma}^{S^T}\boldsymbol{K}^{\delta}\boldsymbol{\Phi}_{\Gamma}^S & \boldsymbol{\Psi}_{\Gamma}^{S^T}\boldsymbol{K}^{\delta}\boldsymbol{\Psi}_{\Gamma}^S \end{bmatrix} \tag{6b}$$

$$\boldsymbol{p}^{\text{syn}} = \begin{Bmatrix} \boldsymbol{p}_{\Phi}^S \\ \boldsymbol{p}_{\Psi}^S \end{Bmatrix} \tag{6c}$$

As indicated in Eq. (6), the mistuned system is described only with the normal modes and the attachment modes of the corresponding tuned system. Because no assumption has been made about mistuning in deriving this reduced-order model, the formulation is entirely general and applicable to any kind of mistuned system. The

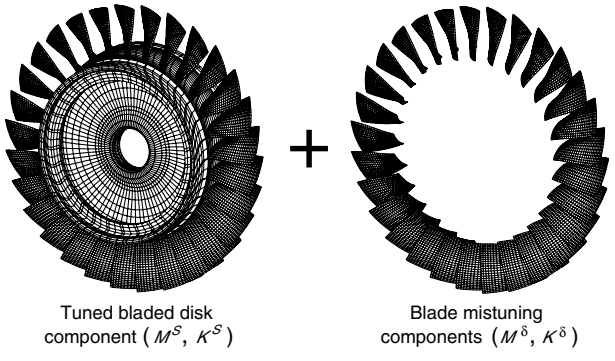

Fig. 1 Substructuring of a mistuned bladed disk.

only restriction is that the number of DOF in a mistuned part must be the same as that in the corresponding part of the tuned system. The number of attachment modes required is the same as the number of DOF of the mistuning components. Although the number of attachment modes may be large (i.e., the number of blade DOF), the attachment modes can be calculated easily and they improve the convergence rate of the natural frequencies and mode shapes of the ROM as the number of tuned-system normal modes increases, as will be discussed in the fourth section. Therefore, an accurate ROM of a reasonable size can be achieved in a systematic manner for arbitrary mistuning by using this general formulation.

Simplified Reduced-Order Model Formulation for Small Mistuning

In this section, the general ROM developed above is simplified by assuming that blade mistuning is small compared to nominal properties in the modal domain, that is, $|(\kappa_{ij}^{\text{syn}} - \kappa_{ij}^{S})/\kappa_{ij}^{S}| \ll 1$. Because the simplified ROM employs mistuning in component modal coordinates of a tuned cantilevered blade, this new technique for small mistuning is called the CMM method.

Approximation for Small Mistuning

Recently, Yang and Griffin reported on modal interaction [29] and applied the results to the modeling of mistuned bladed disks [21]. The main idea for their method is that, when a tuned bladed disk has normal modes closely spaced in a frequency range, a slightly mistuned bladed disk also features closely spaced modes in the same range, and thus the mistuned normal modes can be expressed using a subset of the tuned normal modes. This means that the tuned normal modes outside of the frequency range of interest, or any static modes, can be ignored in modeling a mistuned system with small mistuning.

Using this approach, if $\boldsymbol{\Psi}^{S}$ and the corresponding modal coordinates $\boldsymbol{p}_{\Psi}^{S}$ are ignored in Eq. (6), then the synthesized representation becomes

$$\boldsymbol{\mu}^{\text{syn}} = \left[\boldsymbol{I} + \boldsymbol{\Phi}_{\Gamma}^{S^T}\boldsymbol{M}^{\delta}\boldsymbol{\Phi}_{\Gamma}^{S}\right] \tag{7a}$$

$$\boldsymbol{\kappa}^{\text{syn}} = \left[\boldsymbol{\Lambda}^{S} + \boldsymbol{\Phi}_{\Gamma}^{S^T}\boldsymbol{K}^{\delta}\boldsymbol{\Phi}_{\Gamma}^{S}\right] \tag{7b}$$

$$\boldsymbol{p}^{\text{syn}} = \left\{\boldsymbol{p}_{\Phi}^{S}\right\} \tag{7c}$$

In general, a bladed disk features sets of blade-dominated modes grouped into narrow frequency bands, and the number of normal modes in each band is on the order of the number of blades. Therefore, Eq. (7) provides an accurate representation of a small-mistuned bladed disk in a frequency range of interest with matrices of order N.

It can be observed in Eq. (7) that the mass and stiffness deviation matrices in physical coordinates are projected to the blade portion of the tuned-system normal modes (in this study, mistuning is limited to the blades). Hence, the reduced mass and stiffness matrices can be obtained only if $\boldsymbol{M}^{\delta}$ and $\boldsymbol{K}^{\delta}$ are either known or at least estimated so that they match the mass and stiffness characteristics of the actual blades in a certain frequency range. However, such estimation becomes impractical when $\boldsymbol{M}^{\delta}$ and $\boldsymbol{K}^{\delta}$ are not proportional to the corresponding tuned matrices, which is the case when each blade mode family features a different mistuning pattern.

Component Mode Mistuning Projection

Bladh et al. [15] introduced a mistuning projection method in which the stiffness mistuning matrices in physical coordinates are projected to the normal modes of a tuned blade cantilevered at its root. The projection gives a diagonal matrix of modal stiffness deviations with the assumption that the tuned and mistuned blade-alone mode shapes are the same. With this approach, nonproportional blade mistuning can be implemented efficiently using the modal stiffness deviations, without requiring the estimation of $\boldsymbol{K}^{\delta}$. However, since the ROM is generated by substructuring a rotor into a disk and blades, the model size is larger than that of Yang and Griffin's model [21], which is on the order of the number of blades.

In this section, the blade portion of the tuned-system normal modes in Eq. (7) is represented by a linear combination of boundary modes and selected component modes of a tuned cantilevered blade, with the coefficients referred to as modal participation factors. Using this basis, the mistuning projection method of Bladh et al. [15] can be employed without substructuring the tuned system. Furthermore, it is shown that, even when the mistuning projection matrices are not diagonal, using only the diagonal terms is a good approximation as long as the motion of a blade in a mistuned system is dominated by one mode of a tuned cantilevered blade.

To carry out this projection, the modal participation factors first need to be obtained to represent the blade motion in tuned-system modes. If only cantilevered-blade normal modes are used to describe the blade motion, then the displacements at the boundaries (e.g., disk-blade boundary, shroud-to-shroud boundary) cannot be captured. Therefore, additional modes are required to describe motion at the boundary. However, because it is not feasible to measure these additional boundary modes, the proposed approach is to determine them by minimizing their contribution to the mistuning projection, which is eventually ignored for small boundary displacements.

Here, the additional mode set is introduced in the following form:

$$\begin{bmatrix} \boldsymbol{\Psi}_{o}^{B} \\ \boldsymbol{I} \end{bmatrix}$$

where $\boldsymbol{\Psi}_{o}^{B}$, which is not yet determined, corresponds to the interior DOF of a cantilevered blade, and $\boldsymbol{I}$ corresponds to the boundary DOF that are held fixed in the cantilevered blade model. The number of modes in this set is the number of boundary DOF so that any boundary motion can be described. Because mistuning is usually random, the nominal mass and stiffness matrices of a blade, $\boldsymbol{M}_{o}^{B}$, $\boldsymbol{K}_{o}^{B}$, are used in minimizing the contribution of the boundary modes. Then, the mass and stiffness projections to the boundary modes become

$$\boldsymbol{\mu}_{\psi\psi}^{B} = \begin{bmatrix} \boldsymbol{\Psi}_{o}^{B} \\ \boldsymbol{I} \end{bmatrix}^{T} \begin{bmatrix} \boldsymbol{M}_{ii,o}^{B} & \boldsymbol{M}_{ib,o}^{B} \\ \boldsymbol{M}_{ib,o}^{B^T} & \boldsymbol{M}_{bb,o}^{B} \end{bmatrix} \begin{bmatrix} \boldsymbol{\Psi}_{o}^{B} \\ \boldsymbol{I} \end{bmatrix} \tag{8a}$$

$$\boldsymbol{\kappa}_{\psi\psi}^{B} = \begin{bmatrix} \boldsymbol{\Psi}_{o}^{B} \\ \boldsymbol{I} \end{bmatrix}^{T} \begin{bmatrix} \boldsymbol{K}_{ii,o}^{B} & \boldsymbol{K}_{ib,o}^{B} \\ \boldsymbol{K}_{ib,o}^{B^T} & \boldsymbol{K}_{bb,o}^{B} \end{bmatrix} \begin{bmatrix} \boldsymbol{\Psi}_{o}^{B} \\ \boldsymbol{I} \end{bmatrix} \tag{8b}$$

Now, by taking the first variation of $\boldsymbol{\mu}_{\psi\psi}^{B}$ and $\boldsymbol{\kappa}_{\psi\psi}^{B}$ in $\boldsymbol{\Psi}_{o}^{B}$, the boundary mode contributions to the mass and stiffness projections are minimized, and $\boldsymbol{\Psi}_{o}^{B,m}$ and $\boldsymbol{\Psi}_{o}^{B,k}$ can be obtained from the following equations:

$$\boldsymbol{M}_{ii,o}^{B}\boldsymbol{\Psi}_{o}^{B,m} + \boldsymbol{M}_{ib,o}^{B} = 0 \tag{9a}$$

$$\boldsymbol{K}_{ii,o}^{B}\boldsymbol{\Psi}_{o}^{B,k} + \boldsymbol{K}_{ib,o}^{B} = 0 \tag{9b}$$

Here, it should be noted that $\boldsymbol{\Psi}_{o}^{B,k}$ is the set of Craig–Bampton constraint modes [27] of a cantilevered blade.

Now, the motion of the nth blade in the tuned-system modes is described by cantilevered-blade normal modes and boundary modes as follows:

$$\boldsymbol{\Phi}_{\Gamma,n}^{S} = \begin{cases} \begin{bmatrix} \boldsymbol{\Phi}_{o}^{B} & \boldsymbol{\Psi}_{o}^{B,m} \\ \boldsymbol{0} & \boldsymbol{I} \end{bmatrix} \begin{bmatrix} \boldsymbol{q}_{\phi,n}^{m} \\ \boldsymbol{q}_{\psi,n} \end{bmatrix} & \text{for mass mistuning} \\ \begin{bmatrix} \boldsymbol{\Phi}_{o}^{B} & \boldsymbol{\Psi}_{o}^{B,k} \\ \boldsymbol{0} & \boldsymbol{I} \end{bmatrix} \begin{bmatrix} \boldsymbol{q}_{\phi,n}^{k} \\ \boldsymbol{q}_{\psi,n} \end{bmatrix} & \text{for stiffness mistuning} \end{cases} \tag{10}$$

Therefore, the blade portion of the tuned-system modes can be

expressed as

$$\boldsymbol{\Phi}_{\Gamma}^{S} = \begin{cases} (\boldsymbol{I} \otimes \boldsymbol{U}^{m})\boldsymbol{q}^{m} \\ \text{or} \\ (\boldsymbol{I} \otimes \boldsymbol{U}^{k})\boldsymbol{q}^{k} \end{cases} \tag{11}$$

where

$$\boldsymbol{U}^{m} = \begin{bmatrix} \boldsymbol{\Phi}_{o}^{B} & \boldsymbol{\Psi}_{o}^{B,m} \\ \boldsymbol{0} & \boldsymbol{I} \end{bmatrix} \qquad \boldsymbol{U}^{k} = \begin{bmatrix} \boldsymbol{\Phi}_{o}^{B} & \boldsymbol{\Psi}_{o}^{B,k} \\ \boldsymbol{0} & \boldsymbol{I} \end{bmatrix} \qquad \boldsymbol{q}^{m} = \begin{bmatrix} \vdots \\ \boldsymbol{q}_{\phi,n}^{m} \\ \boldsymbol{q}_{\psi,n} \\ \vdots \end{bmatrix}$$

$$\boldsymbol{q}^{k} = \begin{bmatrix} \vdots \\ \boldsymbol{q}_{\phi,n}^{k} \\ \boldsymbol{q}_{\psi,n} \\ \vdots \end{bmatrix}$$

and $\otimes$ denotes the Kronecker product. Note that since $\boldsymbol{\Psi}_{o}^{B,m}$ and $\boldsymbol{\Psi}_{o}^{B,k}$ are different, $\boldsymbol{q}_{\phi,n}^{m}$ and $\boldsymbol{q}_{\phi,n}^{k}$ are also different. The modal participation factors can be easily calculated because a tuned system is a structure with cyclic symmetry (see the Appendix). In most cases, only a few normal mode participation factors per blade (often just one or two for unshrouded rotors) are dominant, because the blade motion in a tuned-system normal mode tends to be well correlated to that of a cantilevered-blade normal mode (this will be discussed further in the fifth section). Therefore, a few dominant modes are sufficient for the normal mode set, $\boldsymbol{\Phi}_{o}^{B}$.

Inserting Eq. (11) into Eq. (7), the reduced mass and stiffness matrices become

$$\boldsymbol{\mu}^{\text{syn}} = \boldsymbol{I} + \boldsymbol{q}^{mT}(\boldsymbol{I} \otimes \boldsymbol{U}^{mT})\boldsymbol{M}^{\delta}(\boldsymbol{I} \otimes \boldsymbol{U}^{m})\boldsymbol{q}^{m} = \boldsymbol{I} + \sum_{n=1}^{N} \boldsymbol{q}_{n}^{mT}\boldsymbol{U}^{mT}\boldsymbol{M}_{n}^{\delta}\boldsymbol{U}^{m}\boldsymbol{q}_{n}^{m} = \boldsymbol{I} + \sum_{n=1}^{N} \boldsymbol{q}_{n}^{mT}\begin{bmatrix} \boldsymbol{\mu}_{\phi\phi,n}^{\delta} & \boldsymbol{\mu}_{\phi\psi,n}^{\delta} \\ \boldsymbol{\mu}_{\phi\psi,n}^{\delta T} & \boldsymbol{\mu}_{\psi\psi,n}^{\delta} \end{bmatrix}\boldsymbol{q}_{n}^{m} \tag{12a}$$

$$\boldsymbol{\kappa}^{\text{syn}} = \boldsymbol{\Lambda}^{S} + \boldsymbol{q}^{kT}(\boldsymbol{I} \otimes \boldsymbol{U}^{kT})\boldsymbol{K}^{\delta}(\boldsymbol{I} \otimes \boldsymbol{U}^{k})\boldsymbol{q}^{k} = \boldsymbol{\Lambda}^{S} + \sum_{n=1}^{N} \boldsymbol{q}_{n}^{kT}\boldsymbol{U}^{kT}\boldsymbol{K}_{n}^{\delta}\boldsymbol{U}^{k}\boldsymbol{q}^{k} = \boldsymbol{\Lambda}^{S} + \sum_{n=1}^{N} \boldsymbol{q}_{n}^{kT}\begin{bmatrix} \boldsymbol{\kappa}_{\phi\phi,n}^{\delta} & \boldsymbol{\kappa}_{\phi\psi,n}^{\delta} \\ \boldsymbol{\kappa}_{\phi\psi,n}^{\delta T} & \boldsymbol{\kappa}_{\psi\psi,n}^{\delta} \end{bmatrix}\boldsymbol{q}^{k} \tag{12b}$$

where

$$\boldsymbol{\mu}_{\phi\phi,n}^{\delta} = \boldsymbol{\Phi}_{o}^{BT}\boldsymbol{M}_{ii,n}^{\delta}\boldsymbol{\Phi}_{o}^{B} \qquad \boldsymbol{\mu}_{\phi\psi,n}^{\delta} = \boldsymbol{\Phi}_{o}^{BT}\left[\boldsymbol{M}_{ii,n}^{\delta}\boldsymbol{\Psi}_{o}^{B,m} + \boldsymbol{M}_{ib,n}^{\delta}\right]$$

$$\boldsymbol{\mu}_{\psi\psi,n}^{\delta} = \boldsymbol{\Psi}_{o}^{B,mT}\left[\boldsymbol{M}_{ii,n}^{\delta}\boldsymbol{\Psi}_{o}^{B,m} + \boldsymbol{M}_{ib,n}^{\delta}\right] + \boldsymbol{M}_{ib,n}^{\delta T}\boldsymbol{\Psi}_{o}^{B,m} + \boldsymbol{M}_{bb,n}^{\delta}$$

$$\boldsymbol{\kappa}_{\phi\phi,n}^{\delta} = \boldsymbol{\Phi}_{o}^{BT}\boldsymbol{K}_{ii,n}^{\delta}\boldsymbol{\Phi}_{o}^{B} \qquad \boldsymbol{\kappa}_{\phi\psi,n}^{\delta} = \boldsymbol{\Phi}_{o}^{BT}\left[\boldsymbol{K}_{ii,n}^{\delta}\boldsymbol{\Psi}_{o}^{B,k} + \boldsymbol{K}_{ib,n}^{\delta}\right]$$

$$\boldsymbol{\kappa}_{\psi\psi,n}^{\delta} = \boldsymbol{\Psi}_{o}^{B,kT}\left[\boldsymbol{K}_{ii,n}^{\delta}\boldsymbol{\Psi}_{o}^{B,k} + \boldsymbol{K}_{ib,n}^{\delta}\right] + \boldsymbol{K}_{ib,n}^{\delta T}\boldsymbol{\Psi}_{o}^{B,k} + \boldsymbol{K}_{bb,n}^{\delta}$$

Because $\boldsymbol{M}_{n}^{\delta}$ and $\boldsymbol{K}_{n}^{\delta}$ are not necessarily proportional to the nominal matrices, $\boldsymbol{U}^{mT}\boldsymbol{M}_{n}^{\delta}\boldsymbol{U}^{m}$ and $\boldsymbol{U}^{kT}\boldsymbol{K}_{n}^{\delta}\boldsymbol{U}^{k}$ are full matrices, as shown in Eq. (12).

Equation (12) can be used for any small-mistuned bladed disk, but it requires mistuning values for the boundary modes. These values cannot be readily measured, but they can be computed for cases in which the mistuning distribution within the blades is known (e.g., if one assumes proportional mistuning). Now, suppose that the displacements at the boundaries in the tuned-system normal modes are very small, so that the contribution of the boundary modes to the mistuning projection is negligible. This is the usual case for unshrouded rotors. Then, the dominant cantilevered-blade normal modes are sufficient to project mistuning without losing accuracy. In this case, the partitions pertaining to the boundary modes can be ignored and the reduced mass and stiffness matrices can be approximated as

$$\boldsymbol{\mu}^{\text{syn}} \approx \boldsymbol{I} + \sum_{n=1}^{N} \boldsymbol{q}_{\phi,n}^{mT}\boldsymbol{\mu}_{\phi\phi,n}^{\delta}\boldsymbol{q}_{\phi,n}^{m} \tag{13a}$$

$$\boldsymbol{\kappa}^{\text{syn}} \approx \boldsymbol{\Lambda}^{S} + \sum_{n=1}^{N} \boldsymbol{q}_{\phi,n}^{kT}\boldsymbol{\kappa}_{\phi\phi,n}^{\delta}\boldsymbol{q}_{\phi,n}^{k} \tag{13b}$$

Note that $\boldsymbol{\mu}_{\phi\phi,n}^{\delta}$ and $\boldsymbol{\kappa}_{\phi\phi,n}^{\delta}$ still have off-diagonal terms if the mistuned mass and stiffness matrices are not proportional to the nominal matrices. However, each column of $\boldsymbol{q}_{\phi,n}^{m}$ and $\boldsymbol{q}_{\phi,n}^{k}$ is usually dominated by one modal participation factor, and the motion of each blade in a system with small mistuning is usually dominated by one mode of a tuned cantilevered blade. In this case, the off-diagonal terms of $\boldsymbol{\mu}_{\phi\phi,n}^{\delta}$ and $\boldsymbol{\kappa}_{\phi\phi,n}^{\delta}$, which represent the coupling between cantilevered-blade modes due to mistuning, can be neglected. Therefore, Eq. (13) can be simplified further:

$$\boldsymbol{\mu}^{\text{syn}} \approx \boldsymbol{I} + \sum_{n=1}^{N} \boldsymbol{q}_{\phi,n}^{mT}\mathbf{diag}_{r\in\boldsymbol{R}}\left(\mu_{\phi\phi,n,r}^{\delta}\right)\boldsymbol{q}_{\phi,n}^{m} \tag{14a}$$

$$\boldsymbol{\kappa}^{\text{syn}} \approx \boldsymbol{\Lambda}^{S} + \sum_{n=1}^{N} \boldsymbol{q}_{\phi,n}^{kT}\mathbf{diag}_{r\in\boldsymbol{R}}\left(\kappa_{\phi\phi,n,r}^{\delta}\right)\boldsymbol{q}_{\phi,n}^{k} \tag{14b}$$

where

$$\mu_{\phi\phi,n,r}^{\delta} = \boldsymbol{\Phi}_{r,o}^{BT}\boldsymbol{M}_{ii,n}^{\delta}\boldsymbol{\Phi}_{r,o}^{B} \qquad \kappa_{\phi\phi,n,r}^{\delta} = \boldsymbol{\Phi}_{r,o}^{BT}\boldsymbol{K}_{ii,n}^{\delta}\boldsymbol{\Phi}_{r,o}^{B}$$

In this equation, the required number of the modal mistuning values per blade is the number of the retained cantilevered-blade normal modes.

Next, the calculation of the modal mistuning matrices, $\boldsymbol{\mu}_{\phi\phi,n}^{\delta}$ and $\boldsymbol{\kappa}_{\phi\phi,n}^{\delta}$, and their diagonal terms is discussed. Assuming that the mode shapes of the actual (i.e., mistuned) nth cantilevered blade have been measured or computed, the tuned-cantilevered-blade normal modes can be expressed as linear combinations of the mistuned-cantilevered-blade normal modes as follows:

$$\boldsymbol{\Phi}_{o}^{B} = \boldsymbol{\Phi}_{n}^{B}\boldsymbol{v}_{n} \tag{15}$$

where $\boldsymbol{v}_{n}$ is a matrix consisting of the modal participation factors.

The mode orthogonality with respect to the mass and stiffness matrices for the mistuned cantilevered blade is written as follows:

$$\boldsymbol{I} = \boldsymbol{\Phi}_{n}^{BT}\left(\boldsymbol{M}_{ii,o}^{B} + \boldsymbol{M}_{ii,n}^{\delta}\right)\boldsymbol{\Phi}_{n}^{B} \tag{16a}$$

$$\boldsymbol{\Lambda}_{n}^{B} = \boldsymbol{\Phi}_{n}^{BT}\left(\boldsymbol{K}_{ii,o}^{B} + \boldsymbol{K}_{ii,n}^{\delta}\right)\boldsymbol{\Phi}_{n}^{B} \tag{16b}$$

Premultiplying by $\boldsymbol{v}_{n}^{T}$, postmultiplying by $\boldsymbol{v}_{n}$, and using Eq. (15),

$$\boldsymbol{v}_{n}^{T}\boldsymbol{v}_{n} = \boldsymbol{\Phi}_{o}^{BT}\left(\boldsymbol{M}_{ii,o}^{B} + \boldsymbol{M}_{ii,n}^{\delta}\right)\boldsymbol{\Phi}_{n}^{B} = \boldsymbol{I} + \boldsymbol{\mu}_{\phi\phi,n}^{\delta} \tag{17a}$$

$$\boldsymbol{v}_{n}^{T}\boldsymbol{\Lambda}_{n}^{B}\boldsymbol{v}_{n} = \boldsymbol{\Phi}_{o}^{BT}\left(\boldsymbol{K}_{ii,o}^{B} + \boldsymbol{K}_{ii,n}^{\delta}\right)\boldsymbol{\Phi}_{o}^{B} = \boldsymbol{\Lambda}_{o}^{B} + \boldsymbol{\kappa}_{\phi\phi,n}^{\delta} \tag{17b}$$

Therefore,

$$\boldsymbol{\mu}_{\phi\phi,n}^{\delta} = \boldsymbol{v}_{n}^{T}\boldsymbol{v}_{n} - \boldsymbol{I} \tag{18a}$$

$$\boldsymbol{\kappa}_{\phi\phi,n}^{\delta} = \boldsymbol{v}_{n}^{T}\boldsymbol{\Lambda}_{n}^{B}\boldsymbol{v}_{n} - \boldsymbol{\Lambda}_{o}^{B} \tag{18b}$$

The rth diagonal terms of the above mistuning matrices are

$$\boldsymbol{\mu}_{\phi\phi,n,r}^{\delta} = \boldsymbol{v}_{r,n}^{T}\boldsymbol{v}_{r,n} - 1 \tag{19a}$$

$$\boldsymbol{\kappa}^{\delta}_{\phi\phi,n,r} = \boldsymbol{v}^T_{r,n}\boldsymbol{\Lambda}^B_n\boldsymbol{v}_{r,n} - \lambda^B_{r,o} \tag{19b}$$

Because the column vector $\boldsymbol{v}_{r,n}$ is dominated by the factor of the rth mistuned mode $\boldsymbol{v}_{rr,n}$, for small mistuning cases, the diagonal terms can be approximated as

$$\boldsymbol{\mu}^{\delta}_{\phi\phi,n,r} \approx v^2_{rr,n} - 1 \tag{20a}$$

$$\boldsymbol{\kappa}^{\delta}_{\phi\phi,n,r} \approx \lambda^B_{r,n}v^2_{rr,n} - \lambda^B_{r,o} \tag{20b}$$

If only the eigenvalues (or natural frequencies) of the mistuned cantilevered blades are known, then the mass and stiffness mistunings cannot be obtained from the above equation. However, if only stiffness mistuning is assumed, an equivalent stiffness mistuning value $\boldsymbol{\kappa}^{\delta}_{\phi\phi,n,r}$ can be computed. Because no mass mistuning is assumed, $\boldsymbol{\mu}^{\delta}_{\phi\phi,n,r} = 0$, and $v^2_{rr,n} \approx 1$. Then, the equivalent stiffness mistuning value becomes

$$\boldsymbol{\kappa}^{\delta}_{\phi\phi,n,r} \approx \lambda^B_{r,n} - \lambda^B_{r,o} \tag{21}$$

Note that this eigenvalue mistuning was employed in the study by Bladh et al. [15].

Typically, unsteady aerodynamic coefficients are obtained using aerodynamic codes based on a set of cantilevered-blade normal modes in a cyclic assembly (i.e., a cascade) using a complex cyclic coordinate transformation [30]. Therefore, using the cantilevered-blade mode participation factors computed for the mistuning projection in the CMM method, aerodynamic coefficients can also be projected to the normal modes of the tuned system.

Then, the equations of motion for a small-mistuned system with aerodynamic coupling can be expressed as

$$[-\omega^2(\boldsymbol{\mu}^{\text{syn}} + \boldsymbol{\mu}^a) + j\omega\boldsymbol{c}^a + (1 + j\gamma)\boldsymbol{\kappa}^{\text{syn}} + \boldsymbol{\kappa}^a]\boldsymbol{p}^S_\Phi = \boldsymbol{\Phi}^{S^T}\boldsymbol{f} \tag{22}$$

where $\boldsymbol{\mu}^a$, $\boldsymbol{\kappa}^a$, and $\boldsymbol{c}^a$ are the aerodynamic coupling mass, stiffness, and damping matrices in modal coordinates of tuned-system normal modes.

Large Mistuning Case Study: Rogue Blade

The industrial bladed disk depicted in Fig. 1 is used in this study. This integrally bladed rotor (or blisk) has 29 blades, and it is the second stage of a compressor used in an advanced gas turbine application. The rotor model was clamped at the ribs located at the outer edges of the disk, which is a rough approximation of boundary conditions due to neighboring stages. The finite element model was constructed with standard linear brick elements (eight-noded solids), and the total model size was 126,846 DOF.

For a tuned bladed disk, each system mode shape consists of identical motion in each sector except for a fixed sector-to-sector phase difference. Thus, looking at a point in the same relative location in each sector, the mode shapes are sinusoidal in the circumferential direction. This leads to nodal lines across the disk called nodal diameters. Figure 2 displays the free vibration natural frequencies of the tuned bladed disk versus the number of nodal diameters. The natural frequencies and mode shapes were obtained via cyclic symmetry analysis using a finite element model of a single sector. The blade-dominated mode families are labeled on the right-hand side of Fig. 2, where F is a flexural bending mode, T is a torsion mode, S is a stripe or chordwise bending mode, and R denotes elongation in the radial direction. The frequency bounds that will be discussed in the remainder of this paper are marked by dotted horizontal lines in Fig. 2, with the corresponding frequency labeled on the right side.

In this large mistuning case study, a rogue blade scenario was considered in which one blade suffers severe mistuning due to foreign object damage, with all other blades being tuned. Large mistuning was introduced by changing the rogue blade geometry significantly, as depicted in Fig. 3. It was assumed that the mass density and Young's modulus were not changed. Therefore, $\boldsymbol{M}^{\delta}$ and

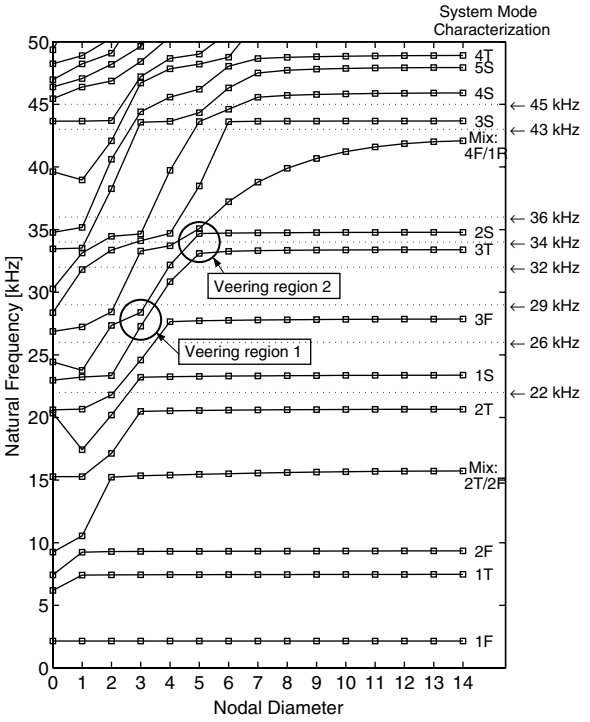

Fig. 2 Natural frequencies versus number of nodal diameters for the tuned rotor FEM.

$\boldsymbol{K}^{\delta}$, which are needed to build the large mistuning ROM, were obtained from the rogue blade geometry. For constructing the ROM, only a single-sector finite element model was required because the attachment modes corresponding to all of the rogue blade DOF were obtained from a cyclic symmetry analysis.

The size of the resulting reduced-order model is equal to the number of kept tuned-system normal modes plus the number of attachment modes. In this case study, a ROM was initially constructed for the frequency range 32–36 kHz (which includes 3T and 2S modes), and the results were compared with those of the finite element model of the full mistuned bladed disk. At a minimum, the tuned-system normal modes in the frequency range of interest were retained, and the attachment modes for all the nodes in the rogue blade were also included. Therefore, the reduced-order model had at least 66 DOF corresponding to the tuned-system modes in the range 32–36 kHz, plus 2496 DOF corresponding to the attachment modes. Although this size is much greater than that of a ROM for small mistuning, it is still much smaller than the parent FEM. Furthermore, a modal analysis could be performed on the reduced-order model to yield a set of normal modes of the mistuned bladed disk. The mistuned-system modes in the range 32–36 kHz could then be selected and used to compute the mistuned forced response.

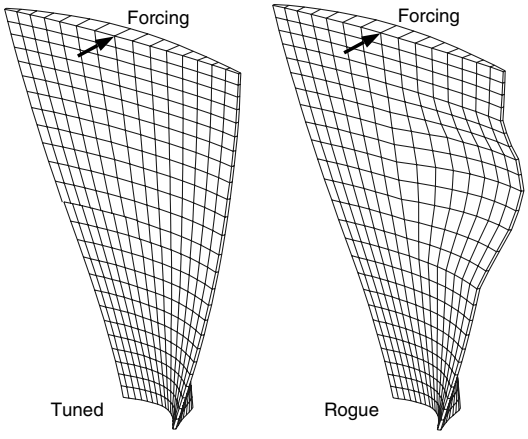

Fig. 3 Rogue blade geometry.

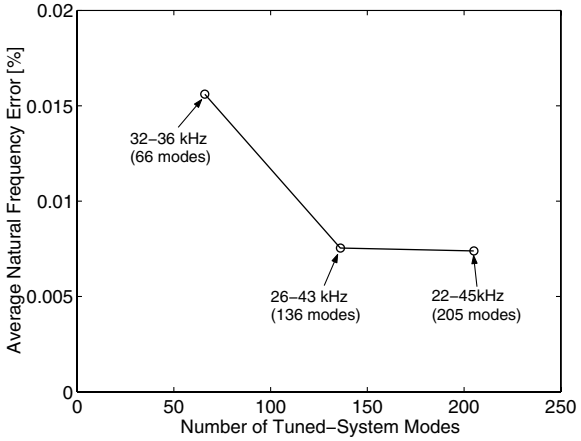

Fig. 4 Convergence of average natural frequency error for the large mistuning case.

To validate the ROM, the convergence of the ROM natural frequencies to the FEM results was examined by increasing the number of tuned-system normal modes. Also, the forced response calculated with the ROM was compared to the FEM results. Figure 4 shows the average natural frequency error versus the number of tuned-system normal modes. The tested frequency ranges for the tuned-system normal mode basis were 32–36 kHz, 26–43 kHz, and 22–45 kHz, and the 66 estimated mistuned natural frequencies that exist between 32 and 36 kHz were chosen for comparison with the FEM results. As can be seen in Fig. 4, the estimated natural frequencies converge to the FEM results as the number of tuned-system normal modes increases. Also, note the very small average error, less than 0.02%, even when the smallest ROM is considered.

Next, the forced response was investigated. From Fig. 4, it is clear that 136 tuned normal modes in the range 26–43 kHz plus the attachment modes are sufficient to describe the behavior of the mistuned system in the range 32–36 kHz, so this ROM was used to compute the forced response. A structural damping coefficient of 0.006 was used. A unit force normal to the blade surface was applied to one of the nodes at the tip of each blade (see Fig. 3), and engine order 1 and 5 excitations were considered. Engine order excitation is the effective traveling wave excitation that a bladed disk experiences as it rotates through the unsteady flow. Thus, the forcing function was assumed to be harmonic in time and differs only in phase from blade to blade. The phase at the nth blade, θ_n, is given by

$$\theta_n = \frac{2\pi C(n-1)}{N} \tag{23}$$

where C is the (integer) engine order of the excitation.

The Euclidean displacement norm was computed for each blade, and the maximum response amplitude of any blade was found at each sampled excitation frequency, so as to provide an envelope of the maximum blade amplitudes versus frequency. The ROM results are shown and compared with the FEM results in Fig. 5. As can be seen, excellent agreement was obtained, thus providing further validation of the ROM's accuracy.

In Fig. 5, note that an additional resonance appears near 34.3 kHz in the response of the mistuned system with the rogue blade, and that this peak is larger than the two resonant peaks for the tuned bladed disk. Hence, the presence of a single rogue blade can significantly alter the forced response, and this effect is accurately captured by the ROM. The other two resonant frequencies of the rogue blade system are almost the same as those of the tuned system, and the peak amplitudes are similar. In the case of engine order 1 excitation, the first main peak corresponds to the 30th mode of the 66 mistuned modes in the 32–36 kHz range, the second peak corresponds to the 36th mode, and the third peak corresponds to the 66th mode. In the case of engine order 5 excitation, the three largest peaks correspond to the 4th, 36th, and 41st modes. These mistuned modes are depicted in Fig. 6 (the displacement of a node at the tip of each blade is shown).

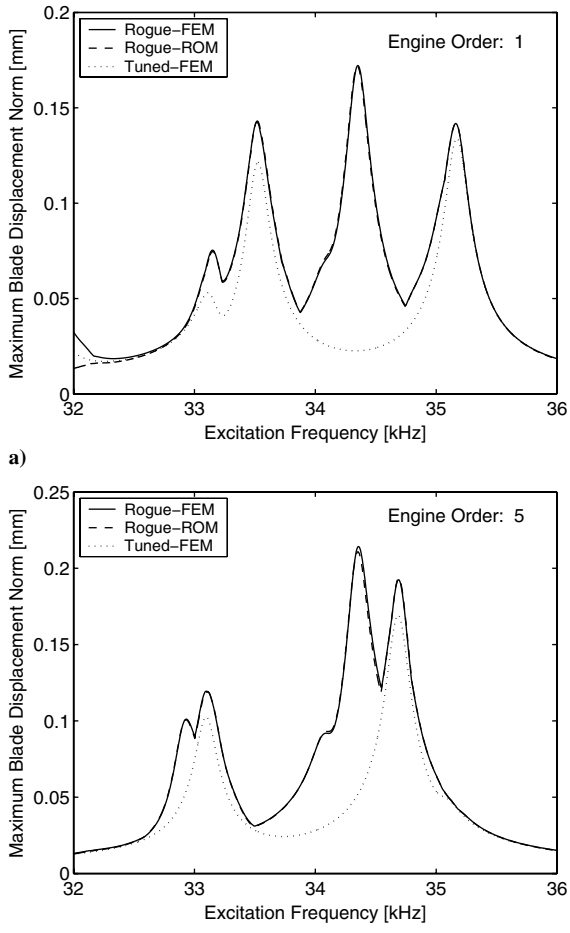

Fig. 5 Forced response results from the FEM (126,846 DOF) and a ROM (2632 DOF) for two cases of engine order excitation.

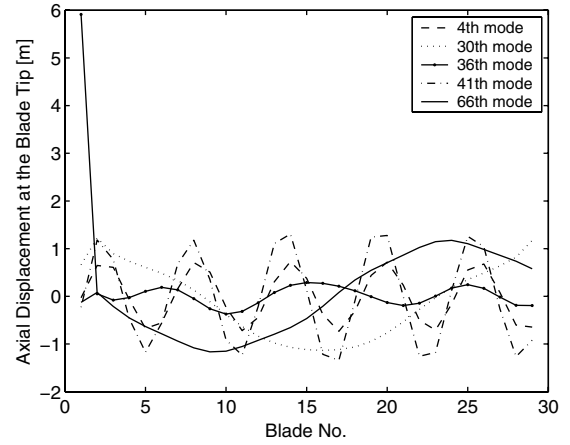

Fig. 6 Five of the 66 mistuned modes in the 32–36 kHz range.

The 30th and 66th modes are nearly sinusoidal waves of harmonic 1 in terms of the blade number, and the 4th and 41st modes are nearly sinusoidal waves of harmonic 5. However, the 36th mode is highly localized to blade 1, which is the rogue blade. Clearly, the largest forced response peak around 34.3 kHz is associated with a rogue-blade-dominated response shape.

Small Mistuning Case Study

To validate the CMM technique for the case of small mistuning, the industrial bladed disk in Fig. 1 was used again. To build a CMM-

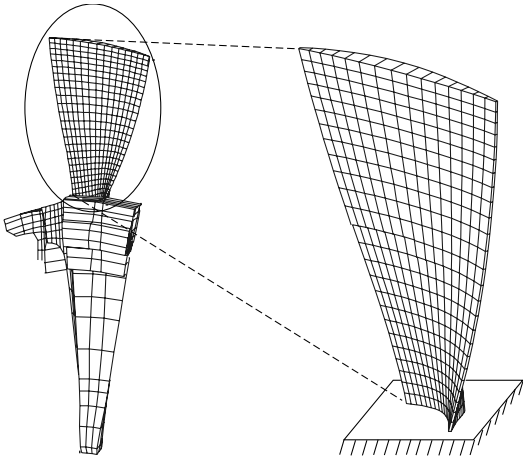

Fig. 7 Single-sector and blade-alone models of an industrial rotor.

based reduced-order model, two tuned finite element models were required, as depicted in Fig. 7:

1) A single-sector model, from which the normal modes of the tuned system were obtained via cyclic symmetry analysis (commercial finite element analysis software packages, such as MSC/NASTRAN, have cyclic symmetry routines). There were 4374 DOF per sector in the finite element model.

2) A blade-alone model, from which the cantilevered-blade normal modes and the static constraint modes were obtained. This model had a total of 2496 DOF, and there were 96 DOF at the interface between the blade and the disk.

The tuned-system normal modes were obtained from the single-sector model. Figure 2 shows the occurrence of numerous natural frequency veering regions. Earlier studies [18,31] have shown that large increases in the mistuned forced response, relative to the tuned response, are likely to occur in veering regions. Therefore, the ability of CMM models to capture the mistuned response in veering regions was tested, and two such regions were investigated: veering region 1 is located at three nodal diameters, around 28 kHz; and veering region 2 is located at five nodal diameters, around 34 kHz. These regions are labeled in Fig. 2.

For this industrial rotor, displacements at the blade root were very small compared to those at the blade's interior, such that the contribution to the mistuning projection of the boundary modes defined at the blade–disk boundary could be neglected. Hence the normal mode mistuning projection used in Eqs. (13) or (14) was sufficient to construct a mistuned ROM. Although the CMM method can handle many types of small blade mistuning, for simplicity mistuning is introduced here as slight variations in the Young's modulus of the blades. That is, only stiffness mistuning was considered, and two cases were investigated: a case of a proportional change in the blade stiffness matrix, and a case of a nonproportional change.

Proportional Mistuning

For a proportional mistuning case, the Young's modulus for blade n was assigned as

$$E_n = E_o(1 + \delta_n^E)$$

where δ_n^E is the mistuning value for blade n. Hence the natural frequencies of all the cantilevered-blade normal modes are mistuned by the same percentage and the mode shapes remain unchanged.

In this case, there are no off-diagonal terms in $\boldsymbol{\kappa}^{\delta}_{\phi\phi,n}$, and only the eigenvalues of the cantilevered blades are mistuned. Hence, Eq. (14) is appropriate for implementing mistuning and $\boldsymbol{\kappa}^{\delta}_{\phi\phi,n}$ becomes exactly $\delta_n^E \boldsymbol{\Lambda}_o^B$. A dimensionless eigenvalue mistuning parameter $\delta^e_{r,n}$ is introduced as

Table 1 Eigenvalue mistuning pattern for the case study rotor with proportional mistuning

Blade	$\delta_n^e\ (=\delta_n^E)$	Blade	$\delta_n^e\ (=\delta_n^E)$
1	0.05704	16	0.04934
2	0.01207	17	0.04479
3	0.04670	18	0.03030
4	−0.01502	19	0.00242
5	0.05969	20	0.01734
6	−0.03324	21	0.02919
7	−0.00078	22	−0.00328
8	−0.01688	23	0.00086
9	0.00242	24	−0.03654
10	−0.02747	25	−0.03631
11	−0.03631	26	−0.01665
12	−0.03570	27	0.00783
13	−0.03631	28	−0.01169
14	−0.03631	29	−0.01332
15	0.00242		

$$\delta^e_{r,n} = \frac{\omega^2_{r,n} - \omega^2_{r,o}}{\omega^2_{r,o}}$$

where $\omega_{r,n}$ is the rth natural frequency of the nth blade and $\omega_{r,o}$ is the rth natural frequency of a tuned blade. For proportional stiffness mistuning, $\delta^e_{r,n}$ is equal to δ_n^E for any mode r, and the eigenvalue mistuning pattern is the same for all blade modes. The specific pattern used to obtain the FEM and CMM results is shown in Table 1.

The CMM model is constructed by selecting a set of tuned-system normal modes to capture mistuned-system normal modes, and a set of cantilevered-blade normal modes to describe the blade motion in the tuned-system normal modes. Because the modal density is high in the investigated veering regions in Fig. 2, a narrow frequency band can be selected for the tuned-system mode basis. For example, 26–29 kHz can be chosen for veering region 1. The selection of cantilevered-blade modes depends on the tuned-system modes chosen for a basis. Namely, modal participation factors for the tuned-system modes in cyclic coordinates need to be calculated using a sufficient number of cantilevered-blade modes [see Eq. (11) and the Appendix], and the dominant cantilevered-blade modes can be determined by comparing the magnitudes of these factors.

Here $\kappa^{\delta}_{\phi\phi,n,r} = \delta^e_{r,n}\omega^2_{r,o}$, and it is pre- and postmultiplied by the corresponding modal participation factors in the mistuning projection. Hence if the levels of random mistuning are on the same order for any mode r, the modal participation factors weighted by the corresponding cantilevered-blade natural frequencies are meaningful in determining what are the dominant cantilevered-blade modes. Figure 8 shows the weighted-average modal participation

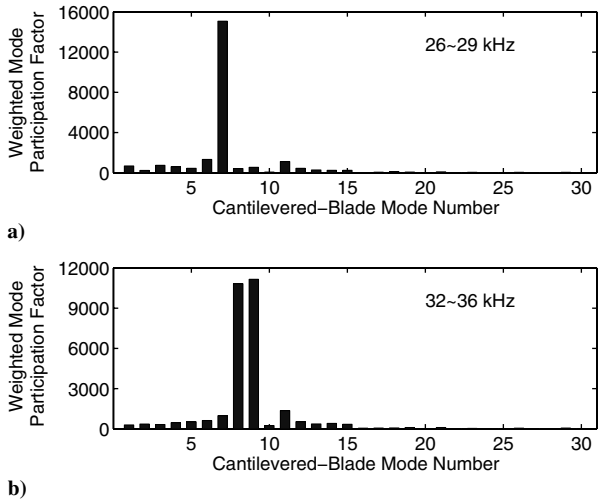

Fig. 8 Weighted-average cantilevered-blade mode participation factors for the blade motion in the tuned-system modes: a) in veering region 1, and b) in veering region 2.

factors, which are defined as

$$\bar{q}^{\,k}_{\phi,r} = \frac{\omega_{r,o} \sum_{h=0}^{H} \sum_{l=1}^{N_h} |\tilde{q}^{k}_{\phi,h,r,l}|}{\sum_{h=0}^{H} N_h} \tag{24}$$

when the lowest 30 cantilevered-blade modes are used to describe the blade motion in the tuned modes in the ranges 26–29 kHz and 32–36 kHz.

It should be noted that the number of cantilevered-blade modes and corresponding mistuning patterns does not affect the size of the ROM, but it can affect its accuracy. Nevertheless, it is desirable to retain a small number of mistuning values, and the dominant cantilevered-blade modes required for accurate mistuning representation can be determined from Fig. 8. For instance, only the seventh cantilevered-blade mode is dominant for the range of 26–29 kHz, because the corresponding weighted-average modal participation factor is much greater than the others. For the same reason, the eighth and ninth modes are dominant for the frequency band of 32–36 kHz. This means that the eigenvalue mistuning patterns for the seventh mode and for the eighth and ninth modes are sufficient to predict the behavior of the mistuned system in the veering regions 1 and 2, respectively.

Once a basis of tuned-system modes is selected and the dominant cantilevered-blade modes are identified for the mistuning projection, a ROM can be built using the CMM technique for the mistuning values in Table 1. Next, the results from the ROM are compared with the FEM results.

The convergence of mistuned natural frequencies and modal assurance criterion (MAC) [23,24] ratios are presented in Figs. 9 and 10 for two frequency bands: 26–29 kHz for region 1, and 32–36 kHz for region 2. Figure 9 shows the average error of the mistuned-system natural frequencies estimated by the CMM model relative to the FEM natural frequencies, versus the number of retained cantilevered-blade modes. Figure 10 shows the average MAC ratio between the CMM and the FEM mistuned modes versus the number of retained cantilevered-blade modes. Because most tuned-system normal modes in the range 26–29 kHz are dominated by the seventh cantilevered-blade mode, the frequency error and MAC ratio are significantly improved when the seventh mode is retained in the CMM model. Similarly, the frequency error and MAC ratio in the range 32–36 kHz show great improvement when the eighth and ninth cantilevered-blade modes are retained. These convergence trends could be predicted from Fig. 8.

The forced response to engine order excitation is considered in the two veering regions indicated in Fig. 2: engine order 3 excitation is applied in region 1, and engine order 5 and 24 excitations are applied in region 2. In both cases, the loads and the structural damping coefficient are the same as for the large mistuning study in the fourth section. The effect of aerodynamic coupling is not considered.

Figures 11 and 12 depict the tuned and mistuned forced response results in veering region 1. In Fig. 11, 34 tuned-system modes (in the range 26–29 kHz) are used, while Fig. 12 is for 106 tuned-system modes (in the range 22–34 kHz). In the case of 34 tuned modes, only the seventh cantilevered-blade mode is employed to project mistuning to the tuned-system modes. In the case of 106 modes, the sixth, seventh, and eighth cantilevered-blade modes are used because these three modes are dominant in the range 22–34 kHz. Note that the largest resonant blade amplitude of the mistuned system is 2.24 times larger than that of the tuned system. In Fig. 11, there are slight differences between the FEM and CMM results for both the tuned and mistuned responses, although for this ROM the average natural

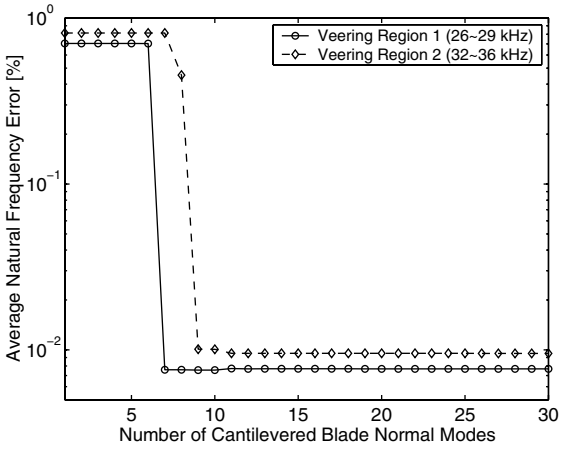

Fig. 9 Convergence of average natural frequency error.

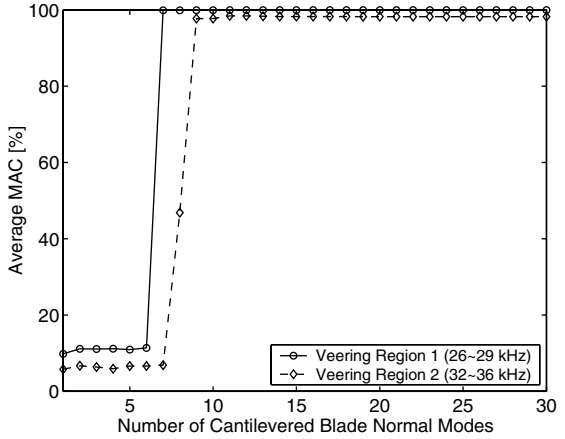

Fig. 10 Convergence of average MAC ratio.

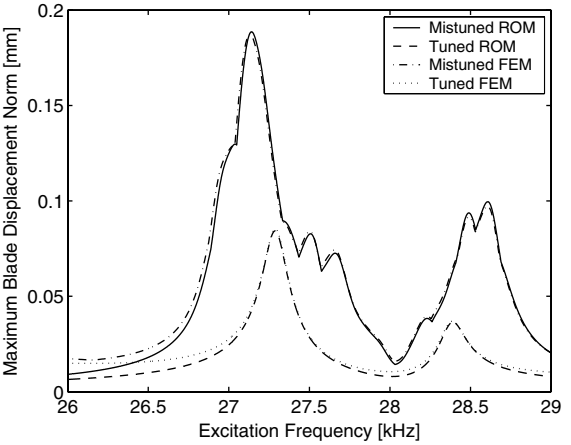

Fig. 11 Frequency response for engine order 3 excitation, obtained by the FEM and a 34-DOF CMM model.

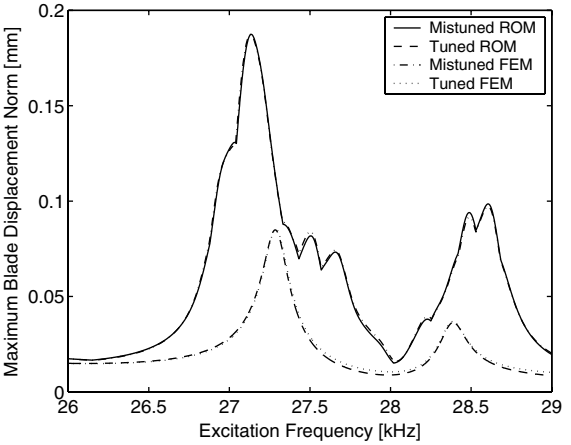

Fig. 12 Frequency response for engine order 3 excitation, obtained by the FEM and a 106-DOF CMM model.

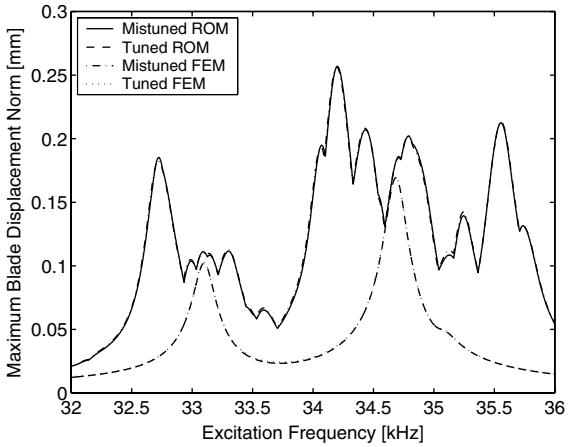

Fig. 13 Frequency response for engine order 5 excitation, obtained by the FEM and a 66-DOF CMM model.

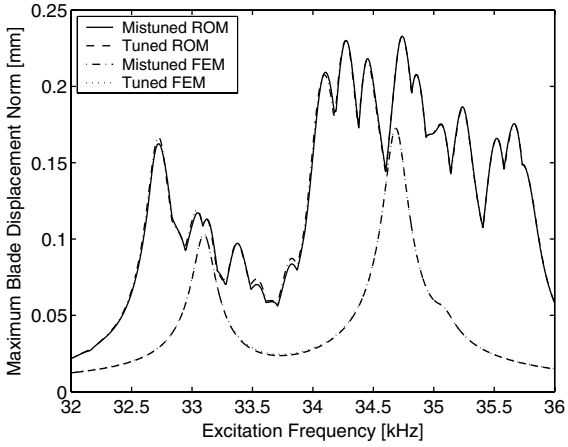

Fig. 14 Frequency response for engine order 24 excitation, obtained by the FEM and a 66-DOF CMM model.

frequency error is only 0.0075% and the average MAC ratio is 99.8958%. This difference can be explained by noting that the mistuned-system modes obtained from the CMM model are in the range 26–29 kHz. Hence, the effects of modes outside this frequency range are not included, and the CMM and FEM results differ even for the tuned response, especially near the edges of the frequency band. As can be seen in Fig. 12, when a wider frequency band is chosen, the discrepancy between FEM and CMM results decreases. But, if one considers the peak amplitudes at resonant frequencies, the 34-DOF CMM model results match the FEM results very closely.

Veering region 2 is more complicated because two close blade-dominated mode families are present in its frequency range. A set of 66 tuned-system modes (32–36 kHz) was used for the CMM modeling, and the eighth (3T) and ninth (2S) cantilevered-blade modes were used for the mistuning projection. Figures 13 and 14 depict forced response results for engine order 5 and 24 excitations, respectively. Note the excellent matches between CMM and FEM results, indicating that the effects of modes outside the 32–36 kHz range are negligible. Also, because the only difference between engine order 5 and engine order 24 excitations for the 29-blade system is the sign of the phase angle of the forcing vector, the tuned forced response is the same in both cases. However, the mistuned forced response results differ for engine orders 5 and 24, and the amplification factors of the largest resonant amplitude are 1.51 and 1.34, respectively.

Nonproportional Mistuning

Here, nonproportional mistuning is considered, and $\boldsymbol{\kappa}^{\delta}_{\phi\phi,n}$ is a full matrix. However, as discussed in the third section, it is a good approximation to use only the diagonal terms of $\boldsymbol{\kappa}^{\delta}_{\phi\phi,n}$, which are approximately the eigenvalue mistuning values. Note that the mistuned blades feature different eigenvalue mistuning patterns for different cantilevered-blade modes. Therefore, the number of mistuning patterns required equals the number of cantilevered-blade modes used in the mistuning projection. Although the mode shapes of cantilevered blades are changed by this type of mistuning, Eq. (14) with only the diagonal mistuning values is employed again, as in the proportional mistuning case. The results are compared with those obtained using Eq. (13) with full mistuning matrices.

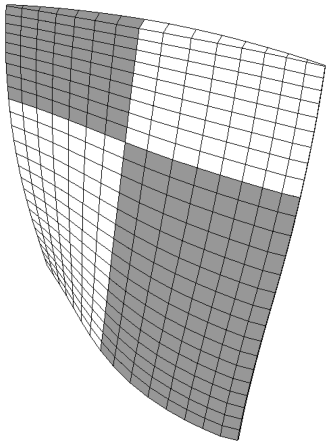

Fig. 15 Illustration of two different Young's modulus values for a blade in the nonproportional mistuning case.

The nonproportional mistuning is introduced by using two different sets of Young's modulus values for the FEM of the cantilevered blades. One ($\delta^{E}_{n,1}$) is for the lower left and upper right parts of blades and the other ($\delta^{E}_{n,2}$) is for the lower right and upper left parts of blades, as illustrated in Fig. 15. The Young's modulus mistuning parameters are listed in Table 2, and Fig. 16 shows the resulting eigenvalue mistuning patterns for several cantilevered-blade modes.

As can be seen in Fig. 16, the eigenvalue mistuning patterns are slightly different from each other. Thus, inaccurate results might be obtained by choosing only one of these patterns, because the dynamic characteristics of a bladed disk can be very sensitive to mistuning. The solution is to use all the mistuning patterns that are available. If there is only one blade-dominated mode family in the frequency band selected for the tuned-system mode basis, as in the case of veering region 1, then a single mistuning pattern may be sufficient. However, if multiple blade-dominated mode families are close and they are included in a reduced-order model, as in the case of veering region 2, then every dominant cantilevered-blade mode should have its own mistuning pattern.

Table 2 Young's modulus mistuning parameters for the case study rotor with nonproportional mistuning

Blade	$\delta^{E}_{n,1}$	$\delta^{E}_{n,2}$	Blade	$\delta^{E}_{n,1}$	$\delta^{E}_{n,2}$
1	0.04080	0.01030	16	0.01990	0.03120
2	−0.06110	−0.04990	17	−0.02490	−0.07530
3	0.01430	0.02780	18	0.06380	0.01350
4	−0.06230	−0.07580	19	0.03140	−0.00080
5	−0.01170	−0.00390	20	−0.01220	−0.00320
6	−0.02700	−0.03210	21	0.03390	−0.01210
7	0.05190	0.00450	22	−0.03220	−0.04590
8	−0.06720	−0.11630	23	−0.00830	0.00530
9	0.03710	0.01770	24	0.06010	0.08270
10	0.06520	0.01460	25	0.02540	0.04540
11	0.06790	0.05580	26	−0.03980	−0.08310
12	0.04000	0.05910	27	0.04700	0.04230
13	−0.00850	−0.05080	28	0.01780	0.01180
14	−0.00020	−0.04850	29	−0.05070	−0.06600
15	−0.03960	−0.02800			

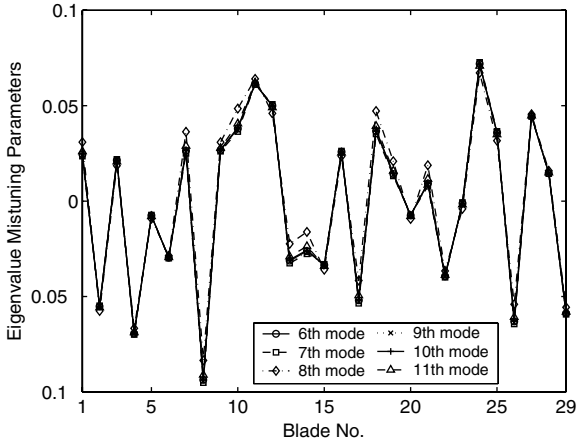

Fig. 16 Mistuning patterns of cantilevered-blade eigenvalues corresponding to modes 6–11 for the case study rotor with nonproportional mistuning.

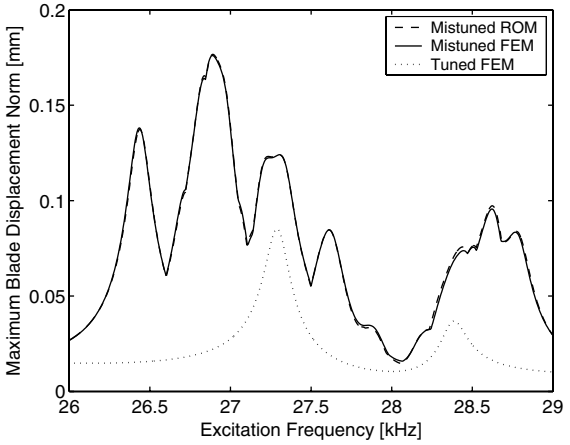

Fig. 17 Frequency response for engine order 3 excitation, obtained by the FEM and the 106-DOF CMM model with the single eigenvalue mistuning pattern of the seventh cantilevered-blade mode applied to the first through 15th cantilevered-blade modes.

These observations are substantiated by investigating the forced response for excitations corresponding to veering regions 1 and 2. In region 1, a single eigenvalue mistuning pattern corresponding to the seventh cantilevered-blade mode has a dominant effect, as in the proportional mistuning case. For the CMM reduced-order model, 106 tuned-system normal modes (22–34 kHz) were retained. Figure 17 shows the forced response in veering region 1 by the FEM and the CMM model. In the CMM model, the eigenvalue mistuning patterns for the first through the 15th cantilevered-blade modes were set to be the same as that of the seventh mode, although they were actually different. As can be seen, the CMM results are in very good agreement with the FEM results. This is because the mistuning pattern for the dominant cantilevered-blade mode is correct.

Figures 18 and 19 show forced response results in the 32–36 kHz range, obtained by four different ROMs and by the FEM. As mentioned earlier, there are two blade-dominated mode groups in this range. In all four cases, 136 tuned-system normal modes (26–43 kHz) were used as a basis, but mistuning projections were performed differently. In Fig. 18a, the single mistuning pattern of the eighth cantilevered-blade mode was used, while in Fig. 18b, the single mistuning pattern of the ninth cantilevered-blade mode is used. For these single mistuning pattern cases, mistuning is projected to the lowest 15 cantilevered-blade modes. In Fig. 19a, the two mistuning patterns of the eighth and ninth cantilevered-blade modes are used to project the mistuning values to the corresponding cantilevered-blade modes, respectively. In Fig. 19b, the six mistuning patterns of the sixth to the 11th cantilevered-blade modes are used in the mistuning projection.

Results show clearly that the ROMs with two and six eigenvalue mistuning patterns predict the mistuned-system response considerably better than those with the single mistuning patterns. In fact, using a single pattern is seen to lead to poor results, including for the resonant response amplitudes. This demonstrates that when multiple blade-dominated mode groups are so close that they interact in the response of a mistuned system, all the eigenvalue mistuning patterns corresponding to the dominant cantilevered-blade modes are needed for an accurate reduced-order model. For a bladed disk with several different eigenvalue mistuning patterns, it can be difficult or impractical to obtain $\boldsymbol{K}^{\delta}$ in physical coordinates, especially if changes in the individual mistuned mode shapes need to be considered. Nevertheless, the CMM technique only requires the eigenvalue mistuning patterns, which can be measured, thus enabling the projection of nonproportional mistuning to tuned-system modes.

Figure 20 shows forced response results for the same frequency range as in Fig. 19. The difference is that the changes in the blade mode shapes due to mistuning were considered, and Eq. (13) was employed. The eigenvalues and mode shapes of the first through 15th cantilevered-blade modes were used, and the full matrices of $\boldsymbol{\mu}^{\delta}_{\phi\phi,n}$ and $\boldsymbol{\kappa}^{\delta}_{\phi\phi,n}$ corresponding to the first through the 15th cantilevered-blade modes were obtained. Note that the eigenvalues and mode shapes were obtained from the finite element models of the mistuned blades. In Fig. 20a, only the mistuning values corresponding to the eighth and the ninth cantilevered-blade modes were used in the ROM, while in Fig. 20b, the mistuning values for the sixth through the 11th cantilevered-blade modes were used. These results are seen to be more accurate than those in Fig. 19, because mode shape

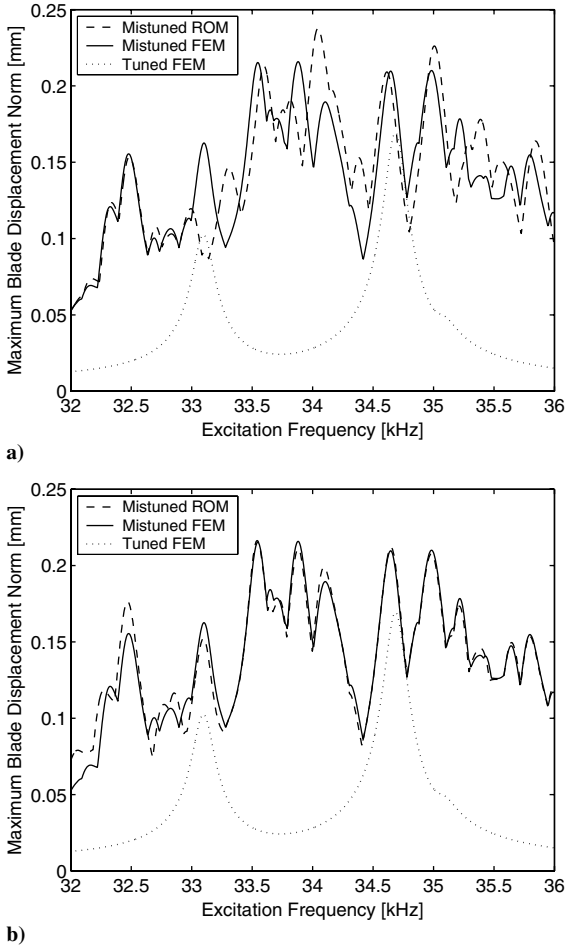

Fig. 18 Frequency response for engine order 5 excitation, obtained by the FEM and 136-DOF CMM models with a single eigenvalue mistuning pattern of a) the eighth and b) the ninth cantilevered-blade mode applied to the lowest 15 cantilevered-blade modes.

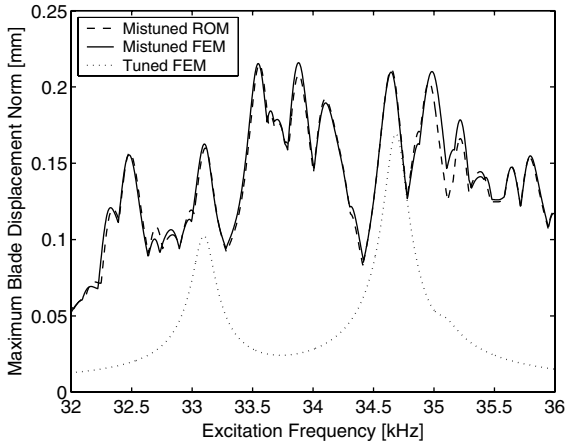

a)

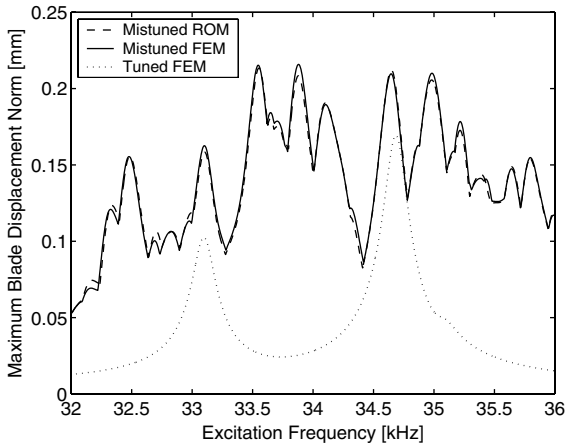

b)

Fig. 19 Frequency response for engine order 5 excitation, obtained by the FEM and 136-DOF CMM models with eigenvalue mistuning patterns of a) the eighth and the ninth, and b) the sixth to 11th cantilevered-blade modes applied to the corresponding cantilevered-blade modes.

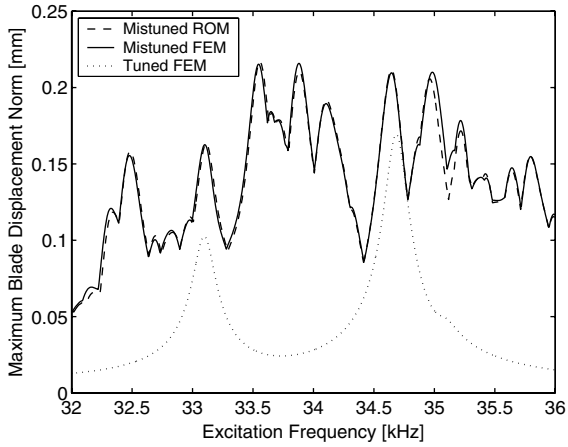

a)

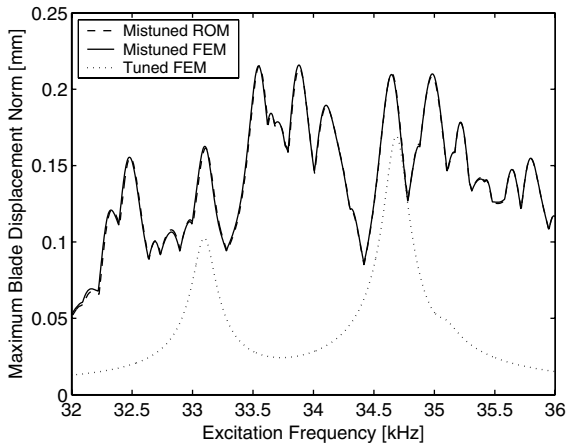

b)

Fig. 20 Frequency response for engine order 5 excitation, obtained by the FEM and 136-DOF CMM models with mistuning values obtained using eigenvalues and mode shapes corresponding to a) the eighth and the ninth, and b) the sixth to 11th cantilevered-blade normal modes.

mistuning was included. Also, the results in Fig. 20b are slightly better than those in Fig. 20a. However, note that the accuracy of the results in Fig. 19, which only includes eigenvalue mistuning, is very good.

Finally, note that the reduced-order modeling framework presented in this paper can be readily applied to shrouded rotors. The interested reader is referred to a previous study by the authors [32].

Conclusions

A general reduced-order modeling framework for mistuned bladed disks was developed by treating a mistuned system as a combination of a tuned-system component and virtual blade mistuning components. This approach handles the case of large blade mistuning, such as geometric blade damage. The method employs tuned-system normal modes and attachment modes to represent mistuned-system normal modes.

A compact ROM for the important case of small blade mistuning was also derived from the general formulation, using a component mode mistuning method. In the CMM method, the finite element models of a tuned sector and a tuned cantilevered blade are required. A linear combination of selected cantilevered-blade normal modes and disk-blade (and possibly shroud–shroud) boundary modes are employed to describe the blade motion of the tuned-system normal modes that are obtained from the single-sector model. Thereby, mistuning values in the modal domain of the cantilevered-blade component modes are projected onto the tuned-system normal modes. The boundary modes are defined by minimizing their contribution in the mistuning projection, and they can be neglected when the tuned-system modes feature displacements at the boundaries that are much smaller than those at the interior of a blade. Therefore, in many cases, modal mistuning values corresponding to a few dominant cantilevered-blade modes are sufficient to predict the response of a mistuned system. The modal mistuning values corresponding to cantilevered-blade modes can be computed easily from the natural frequencies and mode shapes of mistuned blades. This means that actual arbitrary mistuning in the physical domain can be efficiently implemented in a ROM with a small number of mistuning values in the modal domain.

Starting with a finite element model of an industrial turbomachinery rotor, the general ROM was validated for a large mistuning case in which one blade was damaged and featured a significant geometric change from the tuned design. It was observed that the estimated natural frequencies of the mistuned rotor converged rapidly as the selected number of tuned-system modes was increased. Also, the forced response results from the ROM showed excellent agreement with the FEM results.

The CMM method for small blade mistuning was validated for the case in which the mistuned stiffness matrix is proportional to its tuned counterpart, as well as for the nonproportional stiffness mistuning case. For proportional stiffness mistuning, a single eigenvalue mistuning pattern was sufficient for mistuning implementation. For nonproportional mistuning, the mistuning values corresponding to multiple dominant cantilevered-blade modes were required when two blade-dominated mode groups were close. Overall, the CMM method was shown to capture complex mistuning effects with extremely compact ROMs, with the number

of degrees of freedom on the order of the number of blades. Therefore, the CMM method provides tremendous computational savings with good accuracy relative to finite element analysis. Furthermore, compared to previous ROMs, the CMM method is especially useful for predicting mistuned response in higher frequency regions, because 1) there are often many closely spaced blade-dominated mode families; and 2) the blade vibration has shorter wavelength and is more strongly affected by small, local variations in blade properties or geometry.

Appendix: Modal Participation Factors of Cantilevered-Blade Normal Modes

Because a tuned bladed disk features cyclic symmetry, a system mode can be represented by a mode of a single sector in cyclic coordinates and its harmonic number. Therefore, once the modal participation factors for the blade portion of a cyclic single-sector mode are obtained, all the factors for the corresponding full system mode in physical coordinates can be easily computed.

Tuned-system normal modes can be obtained from a single-sector finite element model as

$$\boldsymbol{\Phi}^{S} = (\boldsymbol{F} \otimes \boldsymbol{I}) \underset{h=0,\ldots,H}{\tilde{\mathbf{B}}\mathbf{diag}} \left[\tilde{\boldsymbol{\Phi}}_h^S \right] \tag{A1}$$

where $\tilde{\mathbf{B}}\mathbf{diag}_{h=0,\ldots,H}[\cdot]$ denotes a pseudo-block-diagonal matrix, in which the block sizes can be different, and $\tilde{\boldsymbol{\Phi}}_h^S$ is a real cyclic normal mode set corresponding to harmonic h. In this manner, the blade portion of the tuned-system modes in physical coordinates is expressed as follows:

$$\boldsymbol{\Phi}_{\Gamma}^{S} = (\boldsymbol{F} \otimes \boldsymbol{I}) \underset{h=0,\ldots,H}{\tilde{\mathbf{B}}\mathbf{diag}} \left[\tilde{\boldsymbol{\Phi}}_{\Gamma,h}^S \right] \tag{A2}$$

Next, $\tilde{\boldsymbol{\Phi}}_{\Gamma,h}^S$ is described by cantilevered-blade component modes.

$$\tilde{\boldsymbol{\Phi}}_{\Gamma,h}^{S} = \begin{bmatrix} \tilde{\boldsymbol{\Phi}}_{i,h}^S \\ \tilde{\boldsymbol{\Phi}}_{b,h}^S \end{bmatrix} = \begin{cases} \begin{bmatrix} \boldsymbol{\Phi}_o^B & \boldsymbol{\Psi}_o^{B,m} \\ \mathbf{0} & \boldsymbol{I} \end{bmatrix} \begin{bmatrix} \tilde{\boldsymbol{q}}_{\phi,h}^m \\ \tilde{\boldsymbol{q}}_{\psi,h}^m \end{bmatrix} \\ \text{or} \\ \begin{bmatrix} \boldsymbol{\Phi}_o^B & \boldsymbol{\Psi}_o^{B,k} \\ \mathbf{0} & \boldsymbol{I} \end{bmatrix} \begin{bmatrix} \tilde{\boldsymbol{q}}_{\phi,h}^k \\ \tilde{\boldsymbol{q}}_{\psi,h}^k \end{bmatrix} \end{cases} \tag{A3}$$

where $\tilde{\boldsymbol{q}}_{\phi,h}^m$, $\tilde{\boldsymbol{q}}_{\psi,h}^m$, $\tilde{\boldsymbol{q}}_{\phi,h}^k$, and $\tilde{\boldsymbol{q}}_{\psi,h}^k$ are the participation factors of the cantilevered-blade and boundary modes in the blade portion of the cyclic tuned-system modes of harmonic h. From Eq. (A3), it is obvious that

$$\tilde{\boldsymbol{q}}_{\psi,h}^{m} = \tilde{\boldsymbol{q}}_{\psi,h}^{k} = \tilde{\boldsymbol{\Phi}}_{b,h}^{S} \tag{A4}$$

Before calculating the modal participation factors of the cantilevered-blade modes, it should be noted that the normal modes and the boundary modes of a cantilevered blade are orthogonal with respect to nominal mass and stiffness matrices. This is proved using Eq. (9),

$$\begin{aligned} &\begin{bmatrix} \boldsymbol{\Phi}_o^B \\ \mathbf{0} \end{bmatrix}^T \begin{bmatrix} \boldsymbol{M}_{ii,o}^B & \boldsymbol{M}_{ib,o}^B \\ \boldsymbol{M}_{ib,o}^{BT} & \boldsymbol{M}_{bb,o}^B \end{bmatrix} \begin{bmatrix} \boldsymbol{\Psi}_o^{B,m} \\ \boldsymbol{I} \end{bmatrix} \\ &= \begin{bmatrix} \boldsymbol{\Phi}_o^B \\ \mathbf{0} \end{bmatrix}^T \begin{bmatrix} \boldsymbol{M}_{ii,o}^B \boldsymbol{\Psi}_o^{B,m} + \boldsymbol{M}_{ib,o}^B \\ \boldsymbol{M}_{ib,o}^{BT} \boldsymbol{\Psi}_o^{B,m} + \boldsymbol{M}_{bb,o}^B \end{bmatrix} \\ &= \begin{bmatrix} \boldsymbol{\Phi}_o^B \\ \mathbf{0} \end{bmatrix}^T \begin{bmatrix} \mathbf{0} \\ \boldsymbol{M}_{ib,o}^{BT} \boldsymbol{\Psi}_o^{B,m} + \boldsymbol{M}_{bb,o}^B \end{bmatrix} = \mathbf{0} \end{aligned} \tag{A5a}$$

$$\begin{aligned} &\begin{bmatrix} \boldsymbol{\Phi}_o^B \\ \mathbf{0} \end{bmatrix}^T \begin{bmatrix} \boldsymbol{K}_{ii,o}^B & \boldsymbol{K}_{ib,o}^B \\ \boldsymbol{K}_{ib,o}^{BT} & \boldsymbol{K}_{bb,o}^B \end{bmatrix} \begin{bmatrix} \boldsymbol{\Psi}_o^{B,k} \\ \boldsymbol{I} \end{bmatrix} = \begin{bmatrix} \boldsymbol{\Phi}_o^B \\ \mathbf{0} \end{bmatrix}^T \begin{bmatrix} \boldsymbol{K}_{ii,o}^B \boldsymbol{\Psi}_o^{B,k} + \boldsymbol{K}_{ib,o}^B \\ \boldsymbol{K}_{ib,o}^{BT} \boldsymbol{\Psi}_o^{B,k} + \boldsymbol{K}_{bb,o}^B \end{bmatrix} \\ &= \begin{bmatrix} \boldsymbol{\Phi}^B \\ \mathbf{0} \end{bmatrix}^T \begin{bmatrix} \mathbf{0} \\ \boldsymbol{K}_{ib,o}^{BT} \boldsymbol{\Psi}_o^{B,k} + \boldsymbol{K}_{bb,o}^B \end{bmatrix} = \mathbf{0} \end{aligned} \tag{A5b}$$

Using these orthogonality conditions, $\tilde{\boldsymbol{q}}_{\phi,h}^m$ and $\tilde{\boldsymbol{q}}_{\phi,h}^k$ can be obtained from Eq. (A3) as follows:

$$\begin{aligned} &\begin{bmatrix} \boldsymbol{\Phi}_o^B \\ \mathbf{0} \end{bmatrix}^T \boldsymbol{M}_o^B \tilde{\boldsymbol{\Phi}}_{\Gamma,h}^S = \begin{bmatrix} \boldsymbol{\Phi}_o^B \\ \mathbf{0} \end{bmatrix}^T \boldsymbol{M}_o^B \begin{bmatrix} \boldsymbol{\Phi}_o^B & \boldsymbol{\Psi}_o^{B,m} \\ \mathbf{0} & \boldsymbol{I} \end{bmatrix} \begin{bmatrix} \tilde{\boldsymbol{q}}_{\phi,h}^m \\ \tilde{\boldsymbol{q}}_{\psi,h}^m \end{bmatrix} \\ &= \begin{bmatrix} \boldsymbol{I} & \mathbf{0} \end{bmatrix} \begin{bmatrix} \tilde{\boldsymbol{q}}_{\phi,h}^m \\ \tilde{\boldsymbol{q}}_{\psi,h}^m \end{bmatrix} = \tilde{\boldsymbol{q}}_{\phi,h}^m \end{aligned} \tag{A6a}$$

$$\begin{aligned} &\begin{bmatrix} \boldsymbol{\Phi}_o^B \\ \mathbf{0} \end{bmatrix}^T \boldsymbol{K}_o^B \tilde{\boldsymbol{\Phi}}_{\Gamma,h}^S = \begin{bmatrix} \boldsymbol{\Phi}_o^B \\ \mathbf{0} \end{bmatrix}^T \boldsymbol{K}_o^B \begin{bmatrix} \boldsymbol{\Phi}_o^B & \boldsymbol{\Psi}_o^{B,k} \\ \mathbf{0} & \boldsymbol{I} \end{bmatrix} \begin{bmatrix} \tilde{\boldsymbol{q}}_{\phi,h}^k \\ \tilde{\boldsymbol{q}}_{\psi,h}^k \end{bmatrix} \\ &= \begin{bmatrix} \boldsymbol{\Lambda}_o^B & \mathbf{0} \end{bmatrix} \begin{bmatrix} \tilde{\boldsymbol{q}}_{\phi,h}^k \\ \tilde{\boldsymbol{q}}_{\psi,h}^k \end{bmatrix} = \boldsymbol{\Lambda}_o^B \tilde{\boldsymbol{q}}_{\phi,h}^k \end{aligned} \tag{A6b}$$

Once $\tilde{\boldsymbol{q}}_{\phi,h}^m$ and $\tilde{\boldsymbol{q}}_{\phi,h}^k$ are obtained, $\boldsymbol{q}_{\phi,n}^m$ and $\boldsymbol{q}_{\phi,n}^k$ are expressed using the real Fourier matrix $\boldsymbol{F}$ and the Kronecker product in the same manner as in Eqs. (A1) and (A2). That is,

$$\begin{bmatrix} \vdots \\ \boldsymbol{q}_{\phi,n}^m \\ \vdots \end{bmatrix} = (\boldsymbol{F} \otimes \boldsymbol{I}) \tilde{\mathbf{B}}\mathbf{diag}_{h=0,\ldots,H} \left[\tilde{\boldsymbol{q}}_{\phi,h}^m \right] \tag{A7a}$$

$$\begin{bmatrix} \vdots \\ \boldsymbol{q}_{\phi,n}^k \\ \vdots \end{bmatrix} = (\boldsymbol{F} \otimes \boldsymbol{I}) \tilde{\mathbf{B}}\mathbf{diag}_{h=0,\ldots,H} \left[\tilde{\boldsymbol{q}}_{\phi,h}^k \right] \tag{A7b}$$

Acknowledgment

This work was supported by NASA Grant NAG3-2604, as part of the GUIde Consortium on blade durability at Carnegie Mellon University.

References

[1] Srinivasan, A. S., "Flutter and Resonant Vibration Characteristics of Engine Blades," *Journal of Engineering for Gas Turbines and Power*, Vol. 119, No. 4, 1997, pp. 742–775.

[2] Slater, J. C., Minkiewicz, G. R., and Blair, A. J., "Forced Response of Bladed Disk Assemblies—A Survey," *Shock and Vibration Digest*, Vol. 31, No. 1, 1999, pp. 17–24.

[3] Castanier, M. P., and Pierre, C., "Modeling and Analysis of Mistuned Bladed Disk Vibration: Status and Emerging Directions," *Journal of Propulsion and Power*, Vol. 22, No. 2, 2006, pp. 384–396.

[4] Wagner, J. T., "Coupling of Turbomachine Blade Vibrations Through the Rotor," *Journal of Engineering for Power*, Vol. 89, No. 4, 1967, pp. 502–512.

[5] Dye, R. C. F., and Henry, T. A., "Vibration Amplitudes of Compressor Blades Resulting From Scatter in Blade Natural Frequencies," *Journal of Engineering for Power*, Vol. 91, No. 3, 1969, pp. 182–188.

[6] Ewins, D. J., "The Effects of Detuning Upon the Forced Vibrations of Bladed Disks," *Journal of Sound and Vibration*, Vol. 9, No. 1, 1969, pp. 65–79.

[7] Ewins, D. J., "A Study of Resonance Coincidence in Bladed Discs," *Journal of Mechanical Engineering Science*, Vol. 12, No. 5, 1970, pp. 305–312.

[8] El-Bayoumy, L. E., and Srinivasan, A. V., "Influence of Mistuning on Rotor-Blade Vibrations," *AIAA Journal*, Vol. 13, No. 4, 1975, pp. 460–464.

[9] Griffin, J. H., and Hoosac, T. M., "Model Development and Statistical Investigation of Turbine Blade Mistuning," *Journal of Vibration, Acoustics, Stress, and Reliability in Design*, Vol. 106, No. 2, 1984, pp. 204–210.

[10] Wei, S. T., and Pierre, C., "Localization Phenomena in Mistuned Assemblies with Cyclic Symmetry, Part 1: Free Vibrations," *Journal of Vibration, Acoustics, Stress, and Reliability in Design*, Vol. 110, No. 4, 1988, pp. 429–438.

[11] Wei, S. T., and Pierre, C., "Localization Phenomena in Mistuned Assemblies with Cyclic Symmetry, Part 2: Forced Vibrations," *Journal*

of Vibration, Acoustics, Stress, and Reliability in Design, Vol. 110, No. 4, 1988, pp. 439–449.

[12] Lin, C.-C., and Mignolet, M. P., "An Adaptive Perturbation Scheme for the Analysis of Mistuned Bladed Disks," *Journal of Engineering for Gas Turbines and Power*, Vol. 119, No. 1, 1997, pp. 153–160.

[13] Irretier, H., "Spectral Analysis of Mistuned Bladed Disk Assemblies by Component Mode Synthesis," *Vibrations of Bladed Disk Assemblies: Proceedings of the ASME 9th Biennial Conference on Mechanical Vibration and Noise*, ASME, New York, 1983, pp. 115–125.

[14] Castanier, M. P., Óttarsson, G., and Pierre, C., "A Reduced-Order Modeling Technique for Mistuned Bladed Disks," *Journal of Vibration and Acoustics*, Vol. 119, No. 3, 1997, pp. 439–447.

[15] Bladh, R., Castanier, M. P., and Pierre, C., "Reduced Order Modeling and Vibration Analysis of Mistuned Bladed Disk Assemblies with Shrouds," *Journal of Engineering for Gas Turbines and Power*, Vol. 121, No. 3, 1999, pp. 515–522.

[16] Bladh, R., Castanier, M. P., and Pierre, C., "Component-Mode-Based Reduced Order Modeling Techniques for Mistuned Bladed Disks—Part 1: Theoretical Models," *Journal of Engineering for Gas Turbines and Power*, Vol. 123, No. 1, 2001, pp. 89–99.

[17] Bladh, R., Castanier, M. P., and Pierre, C., "Component-Mode-Based Reduced Order Modeling Techniques for Mistuned Bladed Disks—Part 2: Application," *Journal of Engineering for Gas Turbines and Power*, Vol. 123, No. 1, 2001, pp. 100–108.

[18] Bladh, R., Castanier, M. P., Pierre, C., and Kruse, M. J., "Dynamic Response Predictions for a Mistuned Industrial Turbomachinery Rotor Using Reduced Order Modeling," *Journal of Engineering for Gas Turbines and Power*, Vol. 124, No. 2, 2002, pp. 311–324.

[19] Moyroud, F., Fransson, T., and Jacquet-Richardet, G., "A Comparison of Two Finite Element Reduction Techniques for Mistuned Bladed Disks," *Journal of Engineering for Gas Turbines and Power*, Vol. 124, No. 4, 2002, pp. 942–952.

[20] Yang, M.-T., and Griffin, J. H., "A Reduced Order Approach for the Vibration of Mistuned Bladed Disk Assemblies," *Journal of Engineering for Gas Turbines and Power*, Vol. 119, No. 1, 1997, pp. 161–167.

[21] Yang, M.-T., and Griffin, J. H., "A Reduced Order Model of Mistuning Using a Subset of Nominal System Modes," *Journal of Engineering for Gas Turbines and Power*, Vol. 123, No. 4, 2001, pp. 893–900.

[22] Petrov, E. P., Sanliturk, K. Y., and Ewins, D. J., "A New Method for Dynamic Analysis of Mistuned Bladed Disks Based on the Exact Relationship Between Tuned and Mistuned Systems," *Journal of Engineering for Gas Turbines and Power*, Vol. 124, No. 3, 2002, pp. 586–597.

[23] Allemang, R. J., and Brown, D. L., "A Correlation Coefficient for Modal Vector Analysis," *Proceedings of the 1st International Modal Analysis Conference & Exhibit*, Union College, Schenectady, NY, 1982, pp. 110–116.

[24] Allemang, R. J., "The Modal Assurance Criterion—Twenty Years of Use and Abuse," *Sound and Vibration*, Vol. 37, No. 8, 2003, pp. 14–21.

[25] Castanier, M. P., and Pierre, C., "Using Intentional Mistuning in the Design of Turbomachinery Rotors," *AIAA Journal*, Vol. 40, No. 10, 2002, pp. 2077–2086.

[26] Hurty, W. C., "Dynamic Analysis of Structural Systems Using Component Modes," *AIAA Journal*, Vol. 3, No. 4, 1965, pp. 678–685.

[27] Craig, R. R., Jr., and Bampton, M. C. C., "Coupling of Substructures for Dynamics Analyses," *AIAA Journal*, Vol. 6, No. 7, 1968, pp. 1313–1319.

[28] Craig, R. R., Jr., *Structural Dynamics: An Introduction to Computer Methods*, Wiley, New York, 1981, Chap. 19.

[29] Yang, M.-T., and Griffin, J. H., "A Normalized Modal Eigenvalue Approach for Resolving Modal Interaction," *Journal of Engineering for Gas Turbines and Power*, Vol. 119, No. 3, 1997, pp. 647–650.

[30] Pierre, C., and Murthy, D. V., "Aeroelastic Modal Characteristics of Mistuned Blade Assemblies: Mode Localization and Loss of Eigenstructure," *AIAA Journal*, Vol. 30, No. 10, 1992, pp. 2483–2496.

[31] Kruse, M. J., and Pierre, C., "Forced Response of Mistuned Bladed Disks Using Reduced-Order Modeling," *Proceedings of the 37th AIAA/ASME Structures, Structural Dynamics, and Materials Conference*, Vol. 4, AIAA, Reston, VA, 1996, pp. 1938–1950.

[32] Lim, S., Bladh, R., Castanier, M. P., and Pierre, C., "A Compact, Generalized Component Mode Mistuning Representation for Modeling Bladed Disk Vibration," *Proceedings of the 44th AIAA/ASME/ASCE/AHS Structures, Structural Dynamics, and Materials Conference*, Vol. 2, AIAA, Reston, VA, 2003, pp. 1359–1380; also AIAA Paper 2003-1545.

A. Berman
Associate Editor